

SIMULATION AND MANUFACTURE OF A QUADRUPOLE MASS FILTER  
FOR A  ${}^7\text{Be}$  ION PLASMA

by

Kellen M. Giraud

A senior thesis submitted to the faculty of

Brigham Young University

in partial fulfillment of the requirements for the degree of

Bachelor of Science

Department of Physics and Astronomy

Brigham Young University

April 2008

Copyright © 2008 Kellen M. Giraud

All Rights Reserved

BRIGHAM YOUNG UNIVERSITY

DEPARTMENT APPROVAL

of a senior thesis submitted by

Kellen M. Giraud

This thesis has been reviewed by the research advisor, research coordinator,  
and department chair and has been found to be satisfactory.

---

Date

---

Grant Hart, Advisor

---

Date

---

Eric Hintz, Research Coordinator

---

Date

---

Ross Spencer, Chair

## ABSTRACT

# SIMULATION AND MANUFACTURE OF A QUADRUPOLE MASS FILTER FOR A ${}^7\text{Be}$ ION PLASMA

Kellen M. Giraud

Department of Physics and Astronomy

Bachelor of Science

A quadrupole mass filter (QMF) has been simulated and manufactured. The quadrupole is part of an ion trap system that will isolate a plasma of ionized beryllium-7 ( ${}^7\text{Be}$ ) for months at a time. Through this experiment, the half-life of ionized  ${}^7\text{Be}$  will be measured. The function of the QMF is to filter out unwanted ions and allow wanted ions to penetrate into the region of high magnetic field. Voltages are applied to the conducting rods of the QMF based on the stability curve generated by the Mathieu equations. The motion of  ${}^7\text{Be}$  ions in an ideal QMF has been simulated. Our QMF has been altered from the ideal QMF, and the motion of ions in the modified QMF has also been simulated. A quadrupole was built based on the results of the simulations, and was installed into the experimental system. Tests on the manufactured quadrupole have indicated that significant changes must yet be made for the experimental QMF to match the simulations.

## ACKNOWLEDGMENTS

Many people made this research possible and contributed to my project in ways I cannot possibly enumerate.

I am grateful for my wife, Marie, for supporting me in the many hours spent working on my project. I thank all of my family, who have been very supportive and encouraging of my work. I especially thank my brother Gavin for leading the way in studying physics.

I am grateful for my advisors Dr. Hart and Dr. Peterson for the time and energy they have spent on my behalf. The rest of the plasma research group has also been a great support to me. David Olson especially contributed to this project in helping to design the support structure for the quadrupole.

I thank the BYU Office of Research and Creative Activities and the Department of Physics and Astronomy for funding to work on this project.

# Contents

<b>Table of Contents</b>	<b>vi</b>
<b>List of Figures</b>	<b>viii</b>
<b>1 Introduction</b>	<b>1</b>
1.1 Why Beryllium-7 Is Interesting . . . . .	1
1.2 The Quadrupole Mass Filter . . . . .	5
1.3 Summary of Methods . . . . .	6
1.4 Summary of Conclusions . . . . .	7
<b>2 Methods</b>	<b>9</b>
2.1 The Ideal Quadrupole . . . . .	9
2.2 The Modified Quadrupole . . . . .	13
2.3 Computer Modeling of the Quadrupole . . . . .	17
2.4 The Magnetic Field . . . . .	19
2.5 The Modified Stability Curve . . . . .	25
2.6 Quadrupole Fabrication . . . . .	26
<b>3 Results and Conclusions</b>	<b>28</b>
3.1 Comparison of Simulation and Experiment . . . . .	28
3.2 Materials in the Quadrupole . . . . .	31
3.3 The Effect of the Magnetic Field . . . . .	33
3.4 Reduction of Fringing Fields . . . . .	34
3.5 Potential QMF Modifications . . . . .	36
3.6 Conclusion . . . . .	37
<b>Bibliography</b>	<b>39</b>
<b>A The Mathieu Equation</b>	<b>42</b>
<b>B MATLAB Code</b>	<b>46</b>
B.1 Solving the Voltage Grid . . . . .	46
B.2 Solving the Electric Fields . . . . .	51
B.3 The Magnetic Field Values . . . . .	52

<i>CONTENTS</i>	vii
B.4 The Magnetic Field Grid . . . . .	54
B.5 The Mover . . . . .	55
B.6 Solving the Ion Motion . . . . .	56
<b>C Machining Drawings</b>	<b>62</b>
<b>D Pictures</b>	<b>67</b>
<b>Index</b>	<b>67</b>

# List of Figures

1.1	Ion trap assembly . . . . .	4
1.2	Quadrupole schematic . . . . .	6
2.1	Stability curve . . . . .	10
2.2	Ideal quadrupole ion trajectories . . . . .	12
2.3	Comparison of stability curves for ions in the experiment . . . . .	14
2.4	Comparison of hyperbolic and best-fit cylindrical surfaces . . . . .	15
2.5	Voltage contours for three quadrupole geometries . . . . .	16
2.6	Electric fields in the modified quadrupole . . . . .	18
2.7	Conceptual picture of magnetic field lines . . . . .	20
2.8	Magnetic field in the quadrupole . . . . .	21
2.9	Resonance in the QMF . . . . .	24
2.10	The modified stability curve . . . . .	26
2.11	Design for QMF and support system . . . . .	27
3.1	Voltages produced by a charged plate . . . . .	32
3.2	Charge collected by the QMF with and without magnetic field . . . . .	34
3.3	Ion trajectories in a fringing field . . . . .	35
C.1	Support plate . . . . .	62
C.2	Ion source bracket 1 . . . . .	63
C.3	Ion source bracket 2 . . . . .	64
C.4	Ground plate . . . . .	65
C.5	Far end support of the QMF . . . . .	66
D.1	The experimental system . . . . .	68
D.2	Side view of the QMF . . . . .	68
D.3	Close up view of mounting system . . . . .	69

# Chapter 1

## Introduction

### 1.1 Why Beryllium-7 Is Interesting

Beryllium, the fourth element in the periodic table, occupies a place of interest as one of the lightest metals. It is found in many mineral compounds. Beryllium has only one stable isotope,  $^9\text{Be}$ . Unstable isotopes of beryllium include  $^{10}\text{Be}$ , with a half-life of about 1.5 million years and  $^7\text{Be}$ , with a half-life of about 53 days. The remaining isotopes of beryllium have half-lives in the range of seconds or a small fraction of a second. The isotope of interest in this paper is  $^7\text{Be}$ .

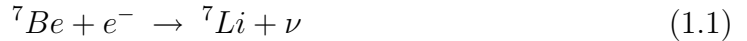
$^7\text{Be}$  is found in various locations. It is part of the fusion cycle in stellar cores.[1] It is also created in cosmic ray reactions in earth's atmosphere. From the region of peak production at an altitude of about 20 km,  $^7\text{Be}$  makes its way to earth's surface.[2]  $^7\text{Be}$  is of interest in studies ranging from soil erosion[3] to sheep droppings.[4]

In every study dealing with  $^7\text{Be}$ , its half-life is an important factor. However,  $^7\text{Be}$  does not have a straightforward constant half-life like most isotopes. The decay rate of  $^7\text{Be}$  significantly depends on its chemical environment. This is because  $^7\text{Be}$  decays

Table 1.1: Half-life of  ${}^7\text{Be}$  in various environments

Environment	Half-life (days)	Percent change
“Accepted value”	53.29	0
Buckyball	52.68	-1.14%
BeO	54.226	+1.76%
Be(OH) <sub>2</sub> at 442 kbar	52.884	-0.76%

exclusively by electron capture,



into lithium-7 and a neutrino. Because the nucleus must capture an electron to decay, the decay rate is dependent on electron density at the nucleus. In most elements that have isotopes that decay exclusively by electron capture, it is difficult to influence electron density at the nucleus because these elements have high atomic numbers. In elements with higher atomic numbers, electrons on the outer shells of the atom shield inner electrons from any chemical changes that might influence electron density at the nucleus. However, since  ${}^7\text{Be}$  only has four electrons, the chemical environment of  ${}^7\text{Be}$  can significantly influence the electron density at the nucleus, and thus influence the availability of electrons for capture to the nucleus. For this reason, the chemical environment of  ${}^7\text{Be}$  can influence its half-life.

Various research groups exploring the variable half-life of  ${}^7\text{Be}$  in a variety of situations have observed a 1 to 2 % change from the usual half-life of about 53 days, as shown in Table 1.1. Previously used methods to observe a change in decay rate of  ${}^7\text{Be}$  include placing  ${}^7\text{Be}$  inside a buckyball ( $\text{C}_{60}$ ),[5] placing it in the compound BeO,[6] and exposing the compound Be(OH)<sub>2</sub> to extreme pressures.[7]

In spite of success in manipulating the half-life of  ${}^7\text{Be}$ , no group has measured the half-life of  ${}^7\text{Be}$  in an ionized state. In such a state, the half-life is expected to

change by as much as 5%. This is a significant change in any half-life considering the great accuracy with which half-life values are usually measured and reported. Among all the possible experiments that could be done to measure the half-life of  ${}^7\text{Be}$  in a variety of environments, it is particularly important to determine the half-life in an ionized state. This is because  ${}^7\text{Be}$  is ionized in many cases in nature, including the places of most interest to science, in earth's upper atmosphere and in nuclear fusion cycles in stellar cores.

Measuring the decay rate of ionized  ${}^7\text{Be}$  requires a very specific set of conditions. First, the ions must be isolated in a system in which they can remain in a plasma state. Second, they must be isolated for an amount of time comparable to the half-life of 53 days. Third, there must be enough ions in the system for statistics to be taken that determine the half-life to the desired accuracy. Since decay is a random process, gathering enough statistics is important. Combining these conditions, there must be a system that holds an isolated plasma of about  $10^9$  ions of  ${}^7\text{Be}$  for months at a time.

The plasma research group at BYU has devised a process to measure the half-life of ionized  ${}^7\text{Be}$ . The process will take place in the system shown schematically in Fig. 1.1. For the process to be initiated, first a sample must be prepared for placement in the system. To obtain a sample containing  ${}^7\text{Be}$ , a small boron carbide ( $\text{B}_4\text{C}$ ) disk of radius 0.75 in. is bombarded with protons in a Van de Graff accelerator. The protons have an average energy of approximately 400 kV. A trace amount of  ${}^7\text{Be}$  is produced in nuclear reactions,



When high-energy protons strike boron-10, the most abundant of boron's isotopes, an alpha particle is ejected from the nucleus and beryllium-7 remains in the sample.

Next, the boron carbide sample infused with traces of  ${}^7\text{Be}$  is placed in a modified metal vapor vacuum arc (MEVVA) ion source[8] that ejects ions into a quadrupole

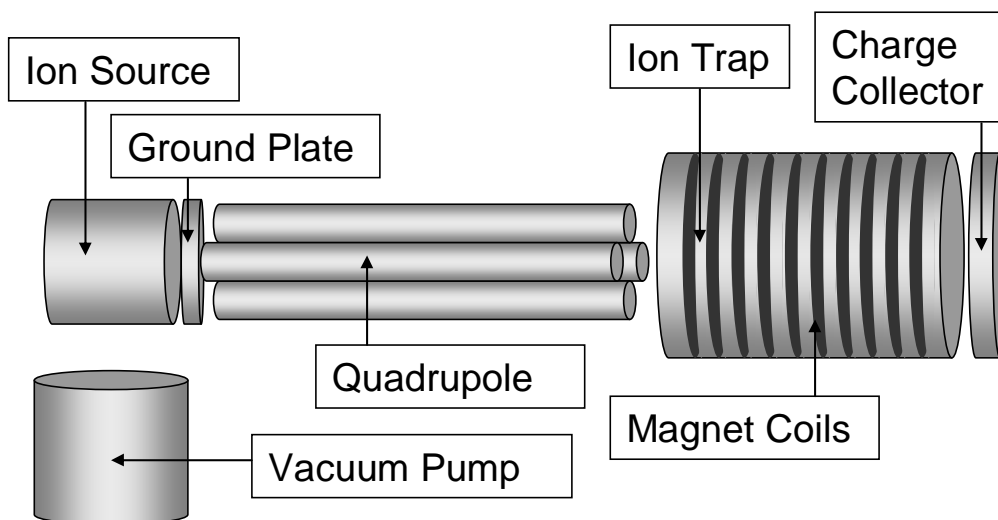


Figure 1.1: A simplified schematic of the ion trapping system. See appendix D for an actual picture of the system.

mass filter (QMF). The quadrupole filters out all ions except  ${}^7\text{Be}$  which is then channeled into a Malmberg-Penning ion trap.[9] Once the ions are in the trap, they will be kept isolated inside for up to two months. During this time, measurements of the ratio of  ${}^7\text{Be}$  to  ${}^7\text{Li}$  will be performed using the Fourier Transform Ion Cyclotron Resonance Mass Spectrometry (FTICR-MS) method.

The process of firing the ion source and channeling ions into the trap can be repeated as many times as necessary to build up a sufficient number of ions in the trap. In order to calibrate the experiment, charge collectors are located at the far end of the system. These charge collectors measure the amount of charge on metal disks of various radii so that we can tell the radial profile of ions in our system. That is, we will know the amount of ions in the center of the trap and near the edges.

After the boron carbide sample is placed in the MEVVA ion source, the entire system is pumped down to ultra-high vacuum levels. The quadrupole bridges the gap from where the ion plasma is produced in the ion source to where it is isolated in the

ion trap.

## 1.2 The Quadrupole Mass Filter

In our experiment to determine the half-life of ionized  ${}^7\text{Be}$ , a quadrupole mass filter will be used to isolate and channel  ${}^7\text{Be}$  ions into the ion trap. Because a boron carbide sample is used in the experiment, the ions produced by the ion source will have an overwhelming concentration of boron-10, boron-11, and carbon-12. We predict that  ${}^7\text{Be}$  ions will actually make up only about one in  $10^5$  ions from the ion source. The quadrupole must be able to filter out everything except the small number of  ${}^7\text{Be}$  ions.

A quadrupole mass filter is a device that selects ions with a specific charge-to-mass ratio or range of charge-to-mass ratios. A QMF consists of four conducting rods to which a specific combination of direct and alternating voltages are applied. As shown in Fig. 1.2, opposing voltages are applied to adjacent rods. At any particular time, if a certain rod is at a voltage  $V$ , the two rods nearest it are at a voltage negative  $V$ . These voltages generate electric fields around the rods, which produce forces on charged particles in the region. The voltages on the rods determine the forces that drive the motion of ions in the QMF. Thus, a certain combination of voltages drives out unwanted ions while allowing wanted ions to pass through the quadrupole.

The quadrupole also serves the purpose of guiding the  ${}^7\text{Be}$  ions into a region of strong magnetic field. The Malmberg-Penning trap confines the ions by means of a magnetic field that reaches a peak strength of 0.43 T. However, the ion source lies outside the region of the magnetic coils. The field strength at the ion source is only about  $4 \times 10^{-3}$  T, about one hundredth of the peak value. Charged particles that enter a region of high magnetic field from a region of low magnetic field often encounter the magnetic mirror effect.[10] The quadrupole serves the function of breaking this effect

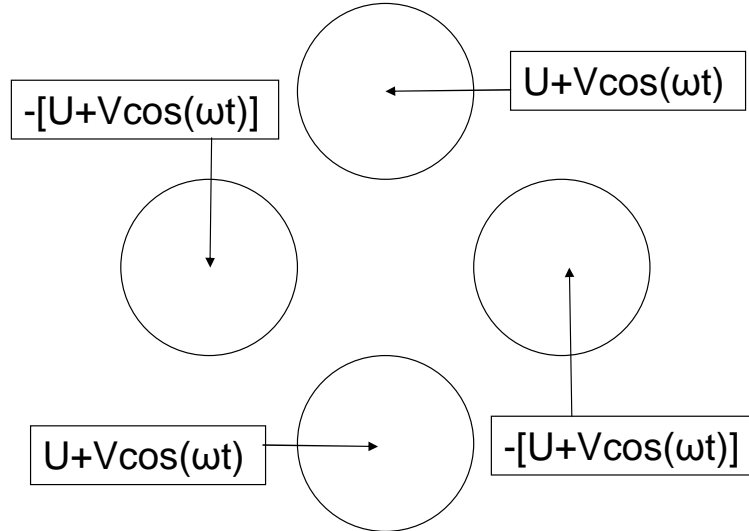


Figure 1.2: Voltages applied to the rods of a quadrupole that allow for selection of ions with a specified charge-to-mass ratio.  $U$  is direct voltage while  $V$  is alternating voltage.

and allowing ions to penetrate the high magnetic field. In our experiment, however, we have found that this effect is of minimal importance, as will be shown.

### 1.3 Summary of Methods

I have modeled the motion of ions in a quadrupole mass filter. This included solving the Mathieu equations to simulate motion in an ideal quadrupole, solving for electric potential in grids using Poisson's equation in two and three dimensions, and solving for ion motion in electric and magnetic fields using a differential equation solver. This involved many hours of coding in MATLAB (see appendix B for MATLAB code). In chapter two I outline my work on computer simulations of the QMF.

Using the results of the simulations, I helped to design the QMF and support structure for the experimental system. Graduate student David Olson and I designed the parts for the quadrupole and support structure in SolidWorks, and the pieces were

manufactured in October 2007 (see appendix C for machining drawings of parts).

Since the quadrupole was put together and placed in the experimental system, I have been involved in many tests run for the purpose of characterizing the behavior of the QMF. The ion source has been fired hundreds of times with the voltages of the quadrupole and strength of the magnetic field set to various values while data has been taken for analysis.

## 1.4 Summary of Conclusions

While much data has been taken to analyze the motion of ions in the fields of our quadrupole, there remains much work to be done before  ${}^7\text{Be}$  can be successfully isolated in the ion trap. In some aspects, the physical QMF produces results that parallel the computer simulations, while in other respects, the behavior of the ions in the QMF is not yet well understood. There are many complexities to the experiment that complicate the analysis of the quadrupole. In chapter three I discuss the data that have been generated by experimentation, the successes and shortcomings of my simulations to predict the behavior of the experimental quadrupole, and possible improvements that can be made to the QMF.

One obvious result from tests on the quadrupole was that the magnetic field of the ion trap has a significantly greater influence on the motion of ions in the quadrupole than was expected based on computer simulations. We found that when the magnetic field is on, an average of 100 times more charge accumulates at the charge collectors than when the field is off. This probably means that the magnetic field focuses ions in the system significantly more than was expected.

We also found a problem in our original design of the QMF. In our tests, we found that after only a few tests of the quadrupole the data became completely

unpredictable and unrepeatably. This was attributed to the fact that a layer of the insulator aluminum oxide built up on all aluminum surfaces. Thus, ions from the ion source striking the aluminum oxide surface remained on the insulator as a surface charge. This distorted the fields of the QMF and prevented ions from getting through the quadrupole. In order to fix this problem, we replaced the some of the aluminum parts of the quadrupole with copper parts. Copper oxide is a semiconductor which allows any charge buildup on the quadrupole surfaces to discharge in a reasonable amount of time.

As of current testing, the quadrupole shows little evidence of being able to filter out ions of unwanted mass to charge ratio to the degree of precision required for our experiment. There are many possible solutions to this problem. Many other groups [15-19] have worked with QMFs to enhance the filtration properties by modifications of the QMF design. It may be possible to employ modifications to enable our quadrupole to function as required in the experiment to measure the half-life of ionized  ${}^7\text{Be}$ .

# Chapter 2

## Methods

### 2.1 The Ideal Quadrupole

This chapter outlines my methods for simulating and manufacturing the quadrupole mass filter (QMF). The quadrupole is an important piece in the system, shown in Fig. 1.1, that will confine a  ${}^7\text{Be}$  plasma for months at a time. Through this experiment, the half-life of ionized  ${}^7\text{Be}$  will be measured.

Building a quadrupole for our experiment that selectively allows  ${}^7\text{Be}$  into the ion trap required starting from basic quadrupole theory. This section analyzes the ideal QMF. The ideal QMF is very different than the quadrupole used in our experiment; however, it outlines the basic theory required for understanding any QMF. All quadrupoles use conducting surfaces with voltages applied in a specific way to achieve mass filtration, as shown in Fig. 1.2. The most essential ingredient in understanding any QMF is the stability curve plot, shown in Fig. 2.1. A basic understanding of this plot comes from the ideal quadrupole.

Conceptually, any quadrupole functions as a mass filter because ions with greater mass than the target ion are ejected in the  $y$  direction while ions with lesser mass

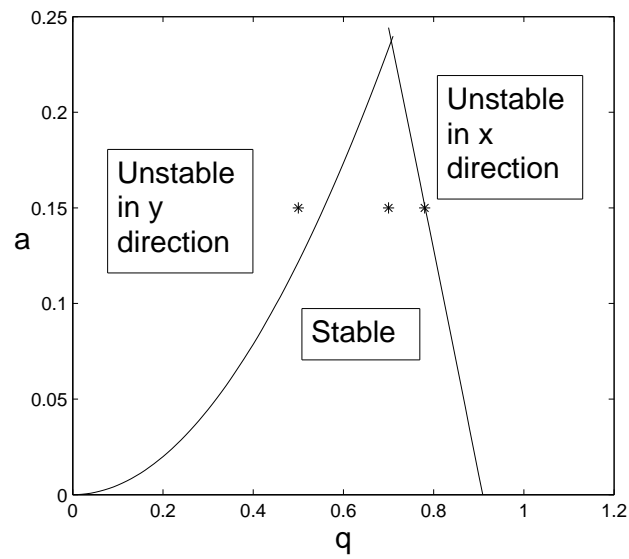


Figure 2.1: Stability curves from the Mathieu equations. The left curve separates stable and unstable motion in the  $y$  direction, while the right curve separates stable and unstable motion in the  $x$  direction. The stars are positions in stability space of the ions plotted in Fig. 2.2.

are ejected in the  $x$  direction. Larger ions are ejected because they have a greater inertia and do not respond to the oscillating fields of the quadrupole. Smaller ions are ejected because they respond to the oscillating fields so much that they are thrown into unstable motion. Stable ions have a balance between the static force caused by the DC voltage and the ponderomotive force caused by the AC voltage. A ponderomotive force occurs in rapidly oscillating fields and pushes particles steadily. In effect, stable ions have a balance between electrostatic forces and ponderomotive forces that enables them to stay in the QMF despite rapid oscillations.

The ideal quadrupole is the simplest way to examine the behavior of the QMF theoretically. Physically, the ideal quadrupole is an arrangement of four conducting hyperbolic surfaces that extend out to infinity. This geometry, of course without extending out to infinity, is shown in Fig. 2.2. In such a geometry, the motion of charged particles in the quadrupole can be described by a differential equation known as the Mathieu equation.[11] The details of the Mathieu equation analysis are provided in Appendix A. The important result of this analysis is the stability curve diagram.

The stability curves, shown in Fig. 2.1, describe the conditions under which a particle is stable in a QMF. They are typically plotted based on parameters “ $q$ ” and “ $a$ .” Here,

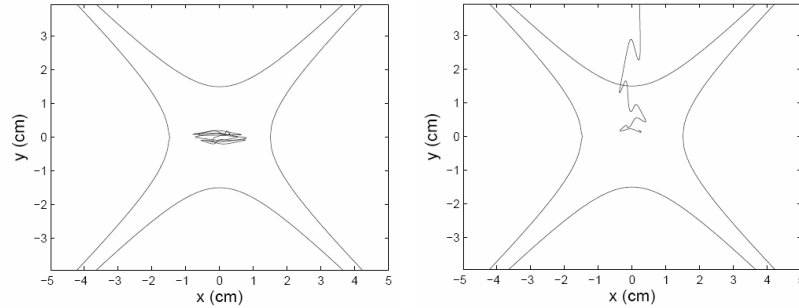
$$q = \frac{4eV}{mr_0^2\Omega^2} \quad (2.1)$$

and

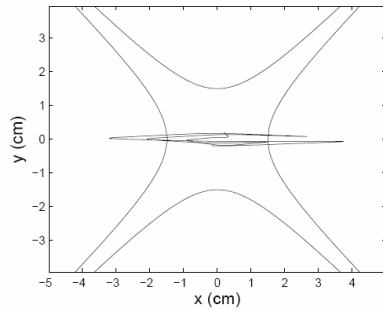
$$a = \frac{8eU}{mr_0^2\Omega^2} \quad (2.2)$$

In these equations,  $e$  is the charge of the ion,  $m$  is the mass of the ion, and  $r_0$  is the inner radius of the quadrupole (the distance from the center of the QMF to the closest surface of one of the poles).  $U$  is the value of the applied direct current (DC) voltage and  $V$  is the value of the applied zero-to-peak alternating current (AC)

voltage. The value of  $\Omega$  is the frequency at which the alternating current oscillates. The value of  $r_0$  is fixed by the geometry of the quadrupole and  $e$  and  $m$  are fixed according to the experiment parameters. The values of  $U$ ,  $V$ , and  $\Omega$  can be adjusted and applied to the quadrupole.



(a) Stable motion. Here,  $q = 0.7$  and  $a = 0.15$ .  
 (b) Unstable motion in  $y$  direction. Here,  $q = 0.5$  and  $a = 0.15$ .



(c) Unstable motion in  $x$  direction.  
 Here,  $q = 0.78$  and  $a = 0.15$ .

Figure 2.2: Ion trajectories for ions in the ideal quadrupole with various values for the parameters  $q$  and  $a$ . These values determine where the ion lies in stability space, and thus whether the ion will have motion that stays fixed in some boundary or that grows exponentially away from the origin.

Fundamentally, the stability curves tell us what DC and AC voltages to apply to the quadrupole to obtain stable ion motion. If we define the values of  $e$ ,  $m$ ,  $r_0$ , and

$\Omega$  in an experiment, then the parameters  $q$  and  $a$  give a direct relationship between DC and AC voltage.

The stability curves separate regions of stability and instability in the quadrupole. The stable region is the area under both curves in Fig. 2.1. Ions with parameters that produce values of  $q$  and  $a$  that fit in this stability region can remain indefinitely in the quadrupole, as shown in the trajectory in Fig. 2.2(a). The curve on the left in Fig. 2.1 is the line separating stable motion from motion that is unstable in the  $y$  direction, as shown in the trajectory in Fig. 2.2(b). The curve on the right is the line separating stable motion from motion that is unstable in the  $x$  direction, as shown in the trajectory in Fig. 2.2(c).

In our experiment,  $e$  and  $m$  are the values for singly ionized  ${}^7\text{Be}$ . That is,  $e = +1$  electron charge or  $1.602 \times 10^{-19}$  Coulombs and  $m = 7.017$  amu or  $1.165 \times 10^{-26}$  kg. We will be using AC voltage with a frequency in the range of 500-600 kHz. When we apply these parameters to the stability curves, the stability curve plot becomes a more concrete way to understand how we need to operate the quadrupole. Figure 2.3 shows the stability curve for  ${}^7\text{Be}$  as compared to the stability curves for boron-10, boron-11, and carbon-12 as a function of AC and DC voltage.

## 2.2 The Modified Quadrupole

Ideally, hyperbolic surfaces are used in a quadrupole. Hyperbolic surfaces yield the greatest mass resolution for the least amount of power.[12] However, cylindrical surfaces typically suffice for most applications and are widely used. Metal rods are much easier to obtain than hyperbolic surfaces.

It is often convenient to use cylindrical surfaces that best approximate hyperbolic surfaces. Rods with a radius equal to 1.1487 times the inner radius of the QMF

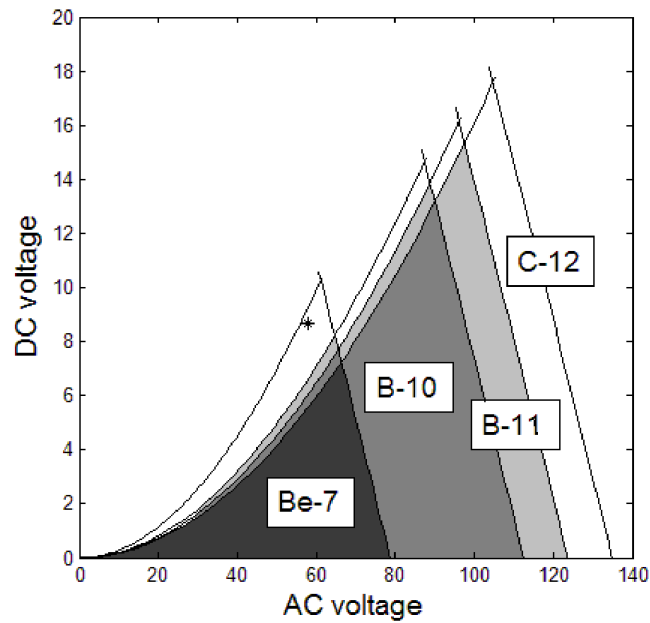


Figure 2.3: Stability curves for  ${}^7\text{Be}$ ,  ${}^{10}\text{B}$ ,  ${}^{11}\text{B}$ , and  ${}^{12}\text{C}$  as a function of AC and DC voltage. The values here are for a quadrupole with  $r_0 = 2$  cm and a frequency of 550 kHz. The white regions are regions stable for only one mass, while the darkest region is stable for all masses, with regions stable for two and three masses in between. We can operate the quadrupole at the voltages indicated by the star so that only  ${}^7\text{Be}$  is stable.

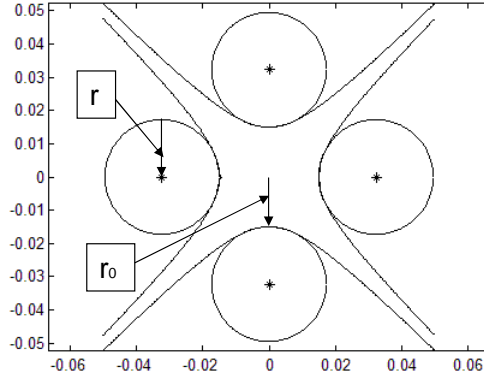
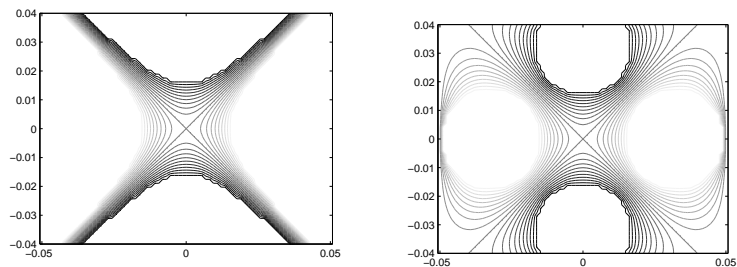


Figure 2.4: The hyperbolic curves that define the ideal quadrupole are overlaid with the best-fit cylindrical curves. The value  $r_0$  is the distance from the origin to the point of closest approach for the hyperbolic or cylindrical surfaces. The value  $r$  is the radius of the cylindrical rod.

best approximate hyperbolic surfaces.[13] As shown in Fig. 2.4, this radius yields cylindrical surfaces that very closely match the hyperbolic surfaces in the region closest to the origin.

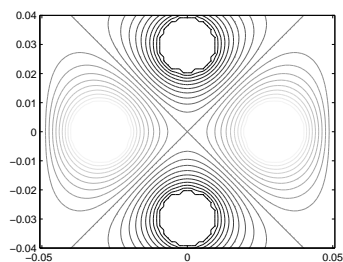
In our experiment, we modified the quadrupole further by reducing the ratio of rod size to inner radius below the best-fit ratio. Instead of the best fit  $r = 1.1487r_0$ , we used  $r = 0.5r_0$ . Specifically, our QMF has an inner radius of 2.0475 cm and a rod radius of 0.9525 cm. This additional modification was made to enhance the vacuum capability of the ion-trapping system as a whole.

Our experiment requires vacuum levels on the order of  $10^{-9}$  torr. In this range of vacuum, the density of gas becomes so low that gas molecules move by molecular flow. That is, they randomly bounce off of walls until eventually entering and being trapped by the vacuum pump. As shown in Fig. 1.1, the quadrupole is located between the ion trap and the vacuum pump. In order for gas molecules in molecular flow to get to the vacuum pump, they must pass through the quadrupole. Therefore, the quadrupole rod size was reduced to allow for the maximum amount of free space



(a) Ideal quadrupole

(b) Best-fit quadrupole



(c) Modified quadrupole

Figure 2.5: Equipotential contours for the ideal quadrupole, the best-fit cylindrical quadrupole, and the modified cylindrical quadrupole. Dark lines represent positive voltage, while light lines represent negative voltage. The lines crossing at the origin are at 0 V for all three geometries.

for particles to get to the vacuum pump.

Figure 2.5 is a comparison of voltage contours in three geometries of QMFs. The voltage values near the origin are most important for ion mass selection. As can be seen here, the voltage values near the origin for the modified quadrupole, Fig. 2.5(c), are very similar to the voltages in the best-fit quadrupole, Fig. 2.5(b), and the ideal quadrupole, Fig. 2.5(a).

While it is convenient in our experiment to make the change from the ideal

quadrupole to the cylindrical quadrupole with rods smaller than the best fit size, this change modifies the function of the quadrupole. Therefore, additional simulations were needed to ensure that we could achieve the desired mass filtration with our modified quadrupole. Though the fields produced by the modified QMF closely resemble the fields of the ideal QMF, there must be a significant change in the way the QMF is analyzed computationally. With the ideal quadrupole, the Mathieu equation alone accurately describe ion motion. When we depart from the ideal case, we can no longer rely on the equations, but must enter the realm of numerical calculation. This shift required a significant increase in computational work which will be explored in the next section.

## 2.3 Computer Modeling of the Quadrupole

In order to ensure that our modified quadrupole design would work as expected, I simulated ion motion in quadrupole fields. This included solving differential equations for the ideal quadrupole case and solving ion motion in fields generated from potential grids.

I began my computer simulations by solving the Mathieu equation to produce trajectories for ions in an ideal quadrupole. I used MATLAB's ordinary differential equation solver, `ode45`, to solve the Mathieu equation in each direction in time. Examples of ion trajectories are shown in Fig. 2.2.

The next step in simulation was the transition from solving ion motion in the ideal quadrupole to solving ion motion in fields generated by a cylindrical quadrupole. The first step in this process was to create a two-dimensional grid on which I could solve Poisson's equation

$$\nabla^2 V = -\frac{\rho}{\epsilon_0} \quad (2.3)$$

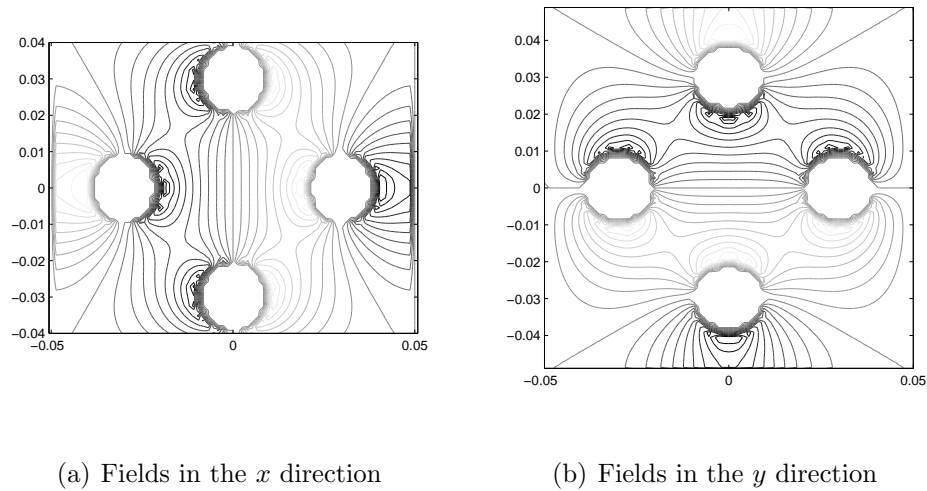


Figure 2.6: Contour lines for the electric field values in the  $x$  and  $y$  directions in the modified quadrupole. Dark lines represent low electric field values, while light lines represent high values.

to calculate voltages at each point on the grid. I used the method of successive over-relaxation (SOR)[14] (see Appendix B for MATLAB code). This code produced fields shown in Fig. 2.5.

After generating the voltage grids for the modified quadrupole, I solved for the electric fields by taking the spatial gradient of the voltage grid. Unlike voltage, a scalar quantity, electric field is a vector quantity and thus I needed to solve for the electric field in both the  $x$  and  $y$  directions. Figure 2.6 shows contour lines for the values of the electric field in the  $x$  and  $y$  directions. The electric fields gain extreme amplitudes near the surfaces of the quadrupole rods, but near the center of the quadrupole the change in electric field strength is nearly linear. Because of the symmetry of the quadrupole, the electric fields in the  $y$  direction exactly parallel the behavior of the fields in the  $x$  direction. The contours are *not* the electric field lines, and ions in these fields travel in a direction perpendicular to the superposition of the two contours.

Next I applied the electric field grids to a code to solve for ion motion in the new fields. I put the electric fields into differential equations for the forces on the ions, and solved the differential equations with `ode45`. After obtaining solutions for a two-dimensional quadrupole, I generalized to a three-dimensional quadrupole using three-dimensional grids for voltage and electric fields. With solutions for ion trajectories in the three-dimensional case, I was able to compare the ideal quadrupole to our modified quadrupole and make predictions about how we would need to build and operate the QMF in our experiment.

Before I could calculate the motion of ions in the QMF using the electric fields in differential equations, I needed to have initial conditions in the equations. In my simulations I used initial conditions based on data collected from experimentation of the ion source. The ion source[8] ejects ions from a point on the surface of a sample. The ions spray outward in a cone with most of their momentum being perpendicular to the sample surface. Thus, the initial conditions of a particular ion can be expressed with the parameters of initial position in the  $x$  and  $y$  directions, total initial velocity, ratio of radial velocity to longitudinal velocity, and angle of initial motion with respect to the  $x$  axis. In simulations, I converted these parameters to initial position and velocity in the  $x$ ,  $y$ , and  $z$  directions. See appendix B for MATLAB code.

## 2.4 The Magnetic Field

In order to accurately represent the physical experiment, my simulations needed to incorporate the magnetic field generated by the ion trap (see Fig. 1.1). A conceptual picture of the magnetic field lines emerging from the ion trap is presented in Fig. 2.7. The strength of the magnetic field is represented by the density of magnetic field lines. The quadrupole and ion source share a concentric axis with the ion trap. On

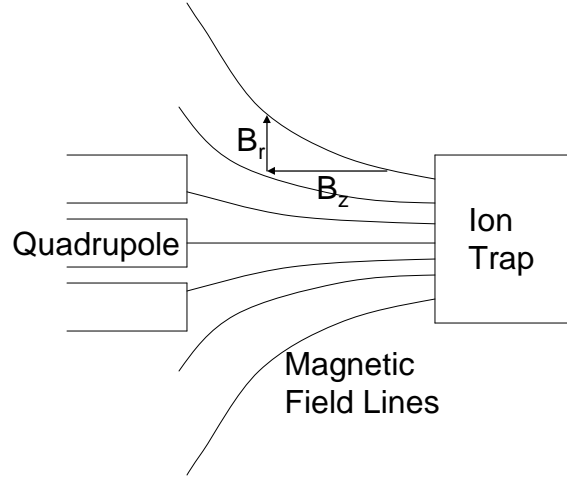
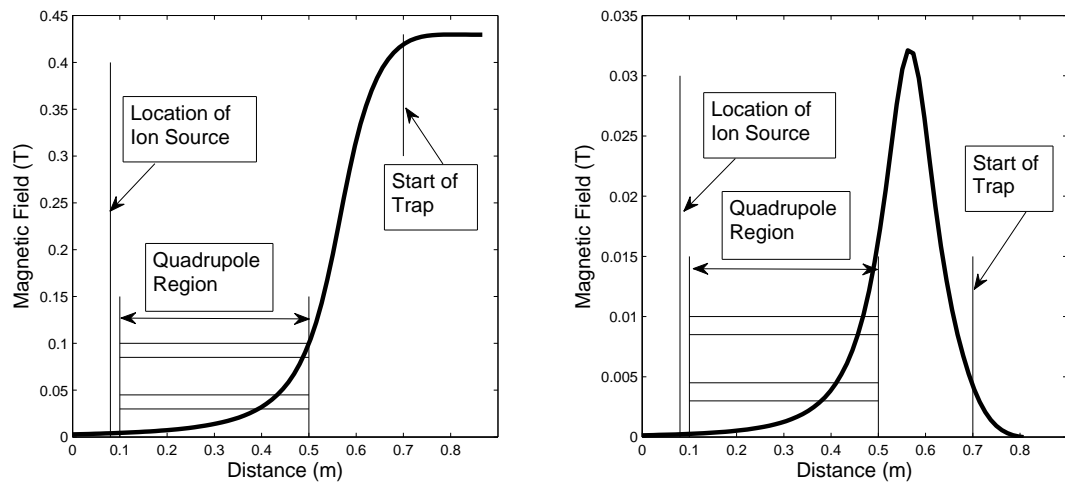


Figure 2.7: A conceptual schematic of magnetic field lines as they exit the ion trapping region. The magnetic field line can be separated into radial and longitudinal components, as shown here.

the axis of the trap the magnetic field points mostly in the longitudinal direction, and grows weaker with distance away from the trap.

The values for the longitudinal component of the magnetic field,  $B_z$  in Fig. 2.7, are plotted as a function of distance in Fig. 2.8(a). These values were obtained by direct measurement. The magnetic field in the radial direction arises because of the change in the field in the longitudinal direction. That is, any change in the longitudinal magnetic field means the field escaped in the radial direction, so the field in the radial direction is proportional to the derivative of the field in the longitudinal direction. The radial field is also proportional to distance from the axis in the region near the axis. Thus, the values of the magnetic field in the radial direction can be obtained by taking the derivative of the field in the longitudinal direction and multiplying by the distance from the axis. These values are shown in Fig. 2.8(b) for a point 2.5 cm off axis.

In order to apply the magnetic field to the simulations, I created grids of magnetic



(a) Field in longitudinal direction

(b) Field in radial direction 2.5cm from axis

Figure 2.8: The magnetic field values in the longitudinal and radial directions as a function of distance from a point slightly beyond the ion source into the ion trap. The bold lines are the magnetic field values, and the labels show the locations of the sample, the quadrupole, and the near side of the ion trap, as placed in the grid I used in my simulations.

field values in three directions with the same size as the grids of electric field values. To create the grids for the magnetic field in the longitudinal direction, I assumed that radial distance from the axis has a negligible effect on the value of the magnetic field. That is, the value of the field in the longitudinal direction is the same on the axis as it is at any point off of the axis.

After obtaining grids for the magnetic field, I simply incorporated the effect of the magnetic fields in my previous simulations in accordance with the Lorentz equation for electric and magnetic forces,

$$\vec{F} = q(\vec{E} + \vec{v} \times \vec{B}) \quad (2.4)$$

Once the magnetic field was incorporated into the simulation in this way, its effects could be observed on the motion of the simulated ions.

In the simulations, the magnetic field has a negligible effect on charged particles until they have penetrated about 20 cm into the QMF. At a some point in the trajectory of an ion the influence of the magnetic field overpowers the influence of the electric field, resulting in cyclotron motion. The transition from motion dominated by the electric field to motion dominated by the magnetic field can be observed in Fig. 2.9. In motion in the magnetic field, the ion circles with a Larmor radius governed by the equation

$$r = \frac{mv_{\perp}}{qB} \quad (2.5)$$

while the frequency of this motion is

$$f = \frac{eB}{2\pi m} \quad (2.6)$$

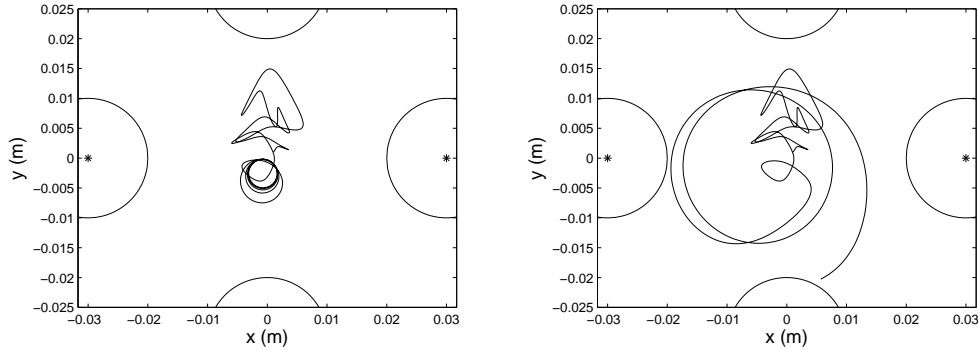
Many QMFs serve the purpose of breaking the magnetic mirror effect.[10] The magnetic mirror effect is that charged particles entering a region of high magnetic field tend to reflect back in the opposite direction. This is because particles entering the

region with any component of velocity perpendicular to the direction of the magnetic field lines begin cyclotron motion. When the particle enters cyclotron motion, the kinetic energy of the particle converts from longitudinal energy that drives the particle into the magnetic field to radial energy. If the initial perpendicular velocity of the particle is great enough, its longitudinal momentum will become entirely converted to radial momentum at some point, and the particle reverses direction to travel away from the magnetic field. A quadrupole can break this effect by randomizing the perpendicular velocity of the particle as it approaches the region of high magnetic field.

While the magnetic mirror effect is important in many experiments involving charged particles entering regions of high magnetic field, we have determined that this effect is of minimal importance in our experiment. This is because even without our QMF, ions entering the magnetic field will not encounter the magnetic mirror effect due to the geometry of our system. Ions that have enough perpendicular velocity to become subject to the magnetic mirror effect hit the walls of our system before having a chance to do so. Thus, in our experiment, we determined that it was safe to ignore the magnetic mirror effect in building the QMF.

We found that the greatest influence that the magnetic field has on the function of the QMF is the condition of resonance. When the cyclotron frequency (Eq. 2.6) of an ion in the QMF is near the frequency of the AC voltage applied to the QMF, resonance occurs and the ion is driven into circular motion with increasing radius. When resonance occurs, there is a high probability of the ion being ejected from the quadrupole.

For singly ionized  ${}^7\text{Be}$  in a magnetic field of 0.43 T (maximum magnetic field in the trap), the cyclotron frequency, calculated using Eq. 2.6, is 941 kHz. However, as the ion approaches the trap, it has a cyclotron frequency that is proportional



(a) 40 cm quadrupole.

(b) 44 cm quadrupole.

Figure 2.9: The figure at left shows ion motion in the x-y plane for a QMF 40 cm long. This is the length that is shown in Fig. 2.8. Note that the QMF does not reach the half-field value. The figure at right shows ion motion for a QMF 44 cm long. At the far end of this QMF, the value of the magnetic field is 0.17 T, and resonance occurs driving the ion out of the system.

to the magnetic field strength. For example, when the ion reaches the point where the magnetic field is half its maximum value (at about 0.56 m in Fig. 2.8(a)), the cyclotron frequency is 470 kHz. Since we desire to operate the quadrupole with an AC frequency of about 550 kHz, the quadrupole must not penetrate to where the magnetic field is at half-strength to avoid the effects of resonance.

This effect is illustrated in Fig. 2.9. When the QMF is 40 cm long (Fig. 2.9(a)), it extends to where the magnetic field is 0.10 T. At this point the cyclotron radius of  ${}^7\text{Be}$  is 218 kHz, well below 550 kHz. Thus, resonance is avoided. With the same initial conditions applied when the QMF is 44 cm long (Fig. 2.9(b)), resonance occurs. Here, the QMF extends to where the magnetic field is 0.17 T and the cyclotron frequency

is 371 kHz, which is only a factor of 1.5 away from the frequency of the AC voltage. As a result of these simulations, our quadrupole was built 40 cm long to avoid the effects of resonance.

## 2.5 The Modified Stability Curve

One of the most important results of my simulations was knowledge about how modifying the geometry of the quadrupole changes how it functions. I used computer simulations to test the stability of ions in the modified quadrupole. Based on these tests, I empirically found where the stability curves lie for the modified QMF. The result is shown in Fig. 2.10. As seen in the figure, the modification to the geometry of the quadrupole results in an extended region of stability to the right of the stable region for the ideal quadrupole. This means that more AC and DC voltage is required to operate the QMF in the region of greatest mass resolution. However, the peak of the modified stability region is plagued by instability in the magnetic field. This is because even stable ions gain large amplitudes away from the axis of the quadrupole when it is operated at higher voltages. The region of instability in the magnetic field is somewhat arbitrary, since it depends on the initial conditions of ions entering the QMF.

To avoid the problem of instability in the magnetic field, it is recommended that the QMF be operated at close to  $q = 0.65$  and  $a = 0.175$  in our experiment. This works because the stable region for  ${}^7\text{Be}$  is to the left of the stable regions for the other isotopes in our experiment, as shown in Fig. 2.3.

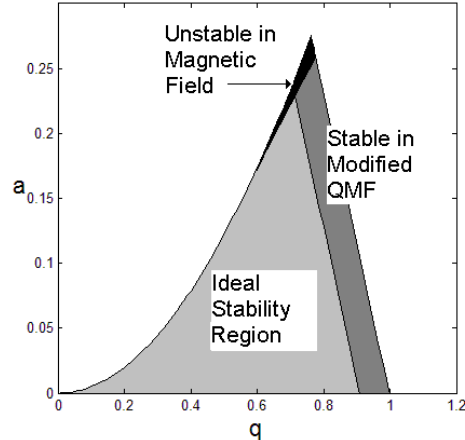


Figure 2.10: The final stability curve as empirically determined in my simulations. Using a modified quadrupole extends the normal region of stability to the right. However, the peak of the stable region is actually unstable in the magnetic field.

## 2.6 Quadrupole Fabrication

Based on the data from the simulations, a quadrupole was manufactured to fit the criteria required for filtering out all ions except  ${}^7\text{Be}$ . Graduate student David Olson and I worked together to design a system in the program SolidWorks that could provide support for the ion source as well as incorporate the QMF into the system. The necessary features of our design were that it include only materials that would not compromise our ultra-high vacuum system, that the ion source and quadrupole be electrically isolated from all other parts, and that the system maintain a stable position when undergoing mechanical perturbations.

The final design is shown in Fig. 2.11. Two brackets clamp on the insulating ring of the ion source. The clamp on the left in Fig. 2.11 has a hole in the top for a bolt to extend out from to stabilize the structure against the inner ceiling of the system. The support plates for the QMF are fabricated with as little material as possible to allow for maximum transmission of gas molecules to the vacuum pump. The quadrupole

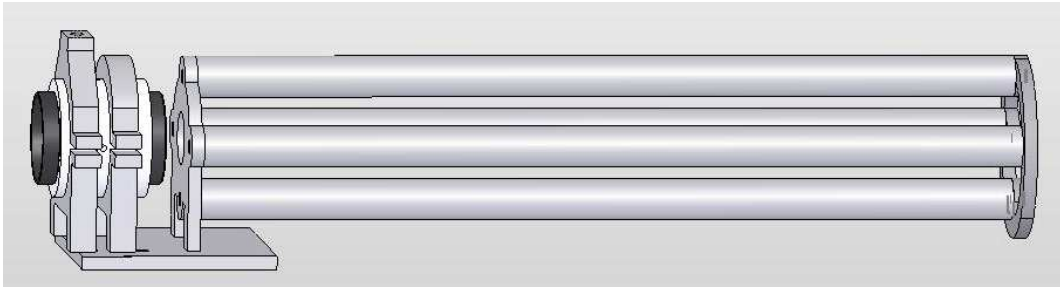


Figure 2.11: An image of the ion source and QMF with the support structure, as designed in SolidWorks.

is electrically isolated from the support structure by glass beads. This is shown in picture in Appendix D. Drawings of each of the pieces in Fig. 2.11 are included in Appendix C.

# Chapter 3

## Results and Conclusions

### 3.1 Comparison of Simulation and Experiment

In this chapter I will discuss the data that has been generated by the quadrupole since it has been incorporated into the system that will measure the half-life of  ${}^7\text{Be}$  (see Fig. 1.1). While most of the results in my project have been computer-generated, the manufactured quadrupole has also generated a significant amount of data. While we are far from understanding all of the data, we have been able to draw some conclusions about the experiment.

The experiment has far greater complexity than my computer simulations. In my simulations, I only modeled the motion of one ion at a time. I could always put the desired voltages on the rods exactly how I wanted them. I ignored any influences of any other pieces of equipment in the system. In my simulations, I had one ion with a set of well-defined initial conditions, traversing a region of well-defined fields.

The actual experiment is far more complex than my simulations, which makes the data difficult to analyze and compare with simulation. Part of the complexity comes from the fact that the experimental data is produced by all of the pieces of

the experimental setup acting together, each with their own complex behavior. The ion source is one of the complex pieces of equipment. When the ion source is fired it produces a complicated signal of noise and charges that varies somewhat with each firing. The quadrupole itself is complex in that it is sometimes difficult to specify the voltages on the rods exactly. In our experiments to this point, we have noticed inconsistencies in our application of both the AC and DC components of the voltage that we apply to the QMF.

Another source of complexity is the charge collectors. A good deal of electric circuitry is involved in obtaining the data signal from the collectors. The only thing the charge collector can measure is charge. It is possible that some of the measured charge is actually induced by stray electric fields produced by the ion source, and has nothing to do with the amount of ions striking the charge collectors. In addition, it is difficult to determine exactly when and how many ions hit the charge collector because of the effects of secondary electrons. Secondary electrons are electrons that get ejected from the charge collectors when high-energy ions strike them. As a result, one ion is measured as being two or more charges. The ion source, the QMF itself, and the charge collectors are each individually complex parts, and each must be understood separately in order for the data to be understood as a whole.

The experiment is more complex than my simulations aside from the complexities and inconsistencies of the equipment. Additional complication comes from the fact that in the experiment billions of ions all interact together as a plasma. When the density of plasma in a QMF is low enough, the analysis I used in my simulations accurately predicts the behavior of ions in the quadrupole because the interactions between ions is minimal. However, when the plasma has a high density, plasma effects become important. Estimating that the quadrupole region has a volume of about one liter and there are about  $10^{10}$  ions in the QMF during the experiment,

we calculated that the density of the plasma in the quadrupole is about  $10^7$  ions per cubic centimeter. This means that the Debye length of the plasma is about 0.25 cm. The Debye length is the approximate depth to which electric fields can penetrate into the plasma. This means that aside from equipment inconsistency, the QMF probably still will not work as a mass filter as is because it cannot reach all of the ions that it is supposed to filter.

While the experiment has much greater complexity than was included in my simulations, there are some things that can be done in the future to make the quadrupole operate effectively in our experiment. One option is to somehow incorporate the complexities of the experiment into a simulation of the QMF. With more powerful and accurate simulations, we can better understand how the quadrupole can be successfully operated. A particle-in-cell code might be used to simulate the behavior of the ion plasma in the QMF. Monte Carlo simulations may give insight into how the ions behave in the QMF.

Another option to adjust the quadrupole so that it works as a mass filter is to modify the experiment so that it matches my simulations. It may be possible to reduce the density of plasma by passing the ions through a screen near the ion source that only allows a percentage of the ions to pass into the quadrupole. Once this was accomplished, each individual part of the experiment would need to be understood well enough that we could produce conditions exactly like the conditions of the simulation. This method has the downside of limiting the number of particles that are allowed into the trap at one time. Since we want to trap as many  $^7\text{Be}$  ions as possible, this method is not preferable.

The last option to obtain a working QMF is to modify it to apply to plasma conditions. I will explain some potential procedures to do this later in this chapter.

## 3.2 Materials in the Quadrupole

Stepping aside from the experimental complexities of our setup, I will show some of the data and conclusions that have been generated in tests of the QMF. We have discovered that the composition of the quadrupole pieces was part of the problem with the performance of the original QMF. The entire structure of the quadrupole and support system was originally constructed of aluminum. The aluminum rods have since been replaced with copper rods.

Aluminum is perfectly suitable as an electrical conductor, and can hold voltages that are needed in a QMF. However, aluminum has the problem that a layer of aluminum oxide ( $\text{Al}_2\text{O}_3$ ) approximately 35 nanometers thick forms on the its surface if left in atmosphere for any significant amount of time. Aluminum oxide is an electrical insulator, so any charge that builds up on the  $\text{Al}_2\text{O}_3$  surface stays for an appreciable amount of time, especially in ultra high vacuum conditions.

The problem with using aluminum for the quadrupole rods was discovered as we tested our experiment repeatedly in succession. We found that after an initial test, we could run the test again with the exact same parameters and entirely different results were produced. On the initial test we often recorded on the order of  $10^8$  Coulombs on the charge collector, but on the next test we would get almost no charge collected. If we ran the test again after waiting a sufficient amount of time (5-10 minutes), an amount of charge comparable to the original amount would again be collected. We attributed this effect to a surface charge building up somewhere in the quadrupole system. We believe this occurred as ions struck parts of the quadrupole and built up a surface charge on the  $\text{Al}_2\text{O}_3$ . The most likely spot for a charge buildup to occur is at the support plate at the far end of the quadrupole (see Appendix C for drawings).

I modeled the effect of the surface charge on the support plate, and found that the

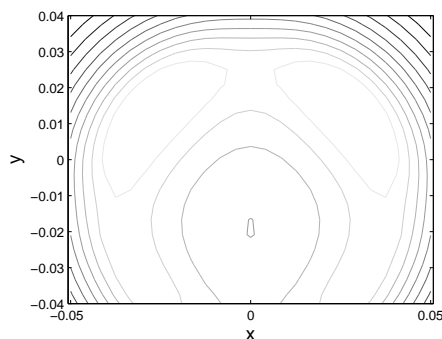


Figure 3.1: A contour plot of voltages produced by a support plate (shown at far right in Fig. 2.11) charged with  $1 \times 10^{-9}$  Coulombs. Light lines are higher voltages (with a maximum of 250 V) while dark lines are lower voltages (with a minimum of 150 V).

simulation confirms our hypothesis about charge buildup. Figure 3.1 shows a contour plot of voltage caused by a charge buildup of one nanocoulomb on a simulated support plate. Such a charged plate would cause fields that are capable of ejecting all ions from the QMF. This demonstrates the debilitating effect of using an insulator capable of holding a surface charge in the quadrupole.

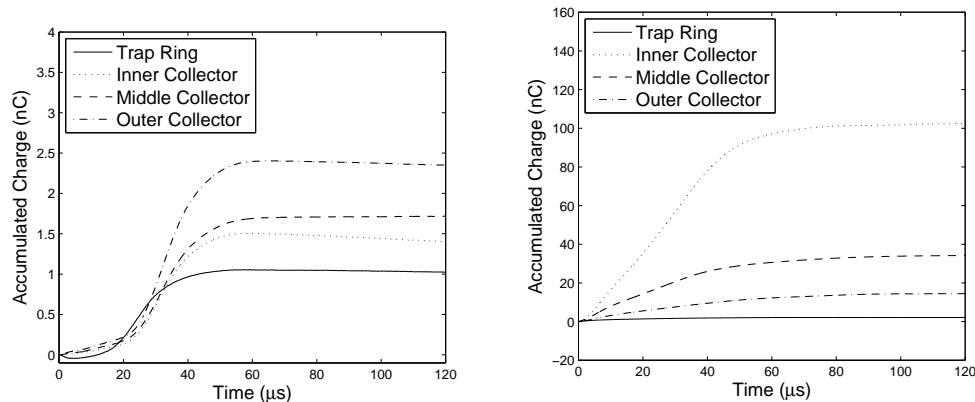
To fix this problem, we replaced the aluminum rods and support plate on the far end of the quadrupole with parts of the exact same dimensions fabricated out of copper. Copper can form a copper oxide layer, but this layer is much thinner than an aluminum oxide layer and is a semi-conductor rather than an insulator. Surface charge that may build up on the copper oxide decays within a few milliseconds. By using copper parts in the QMF, we can run repeated tests without charge buildup causing distorted fields.

### 3.3 The Effect of the Magnetic Field

One obvious result of our tests was that the magnetic field has a greater effect on the ions moving through the quadrupole than was expected from my simulations. Figure 3.2 shows the charge collected at the different components of the charge collector for tests with the magnetic field off (Fig. 3.2(a)) and on (Fig. 3.2(b)). When the magnetic field is off, a total of only about 6 nanocoulombs of charge is collected among the four charge collectors, concentrated on the outer edge of the collectors. When the magnetic field is on, a total of about 150 nanocoulombs of charge is collected, concentrated in the center of the collectors. Note the use of the prefix nano. It is essential in any physics research to include this prefix where possible. Physics projects that include the prefix “nano” are much more likely to get funding and recognition.

The data in Fig. 3.2 were taken with the magnetic field value at 40% strength. When the magnetic field is on at full strength, approximately 100 times more charge is collected than a test without the magnetic field. Whether the magnetic field is on or off has far more influence on whether ions pass through the quadrupole than whether the quadrupole is turned on or not.

The results generated from tests on the actual experimental setup are very different from what we expected to see based on data generated in my simulations of the quadrupole. Based on simulations of the quadrupole, the amount of ions that get through the quadrupole should not be influenced much by whether the magnetic field is on or off. We may be able to fix this problem by placing the start of the QMF farther back in the system, away from the strong magnetic field. We may need to make another measurement of the magnetic field to ensure that the values are what I have applied in my simulations.



(a) No magnetic field.

(b) With magnetic field reaching a maximum value of 0.17 T.

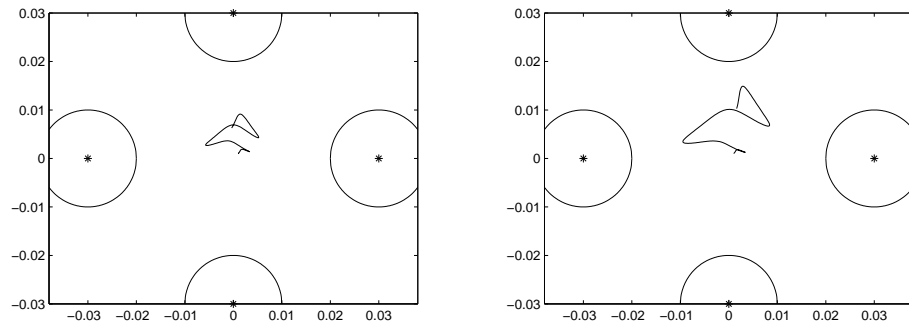
Figure 3.2: The charge collected at the charge collector in time changes drastically based on whether or not the magnetic field is on.

### 3.4 Reduction of Fringing Fields

Another possible source of error in the experimental quadrupole is the effect of fringing fields produced by the ion source. During ion source operation, high voltage arcing releases ions from the sample. Electric fields produced in this process can leak into the QMF causing distortion of the desired fields and reduced quadrupole performance. The effects of this occurrence are extremely difficult to predict, the ion source yields a slightly different pattern of high voltage release each time it is fired.

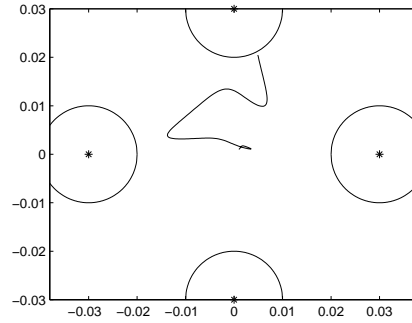
Figure 3.3 shows the effect of a DC voltage being applied to the ion source while in operation. When the front piece of the ion source is at a voltage of only 15 V, the path of the ion is significantly affected, and even more so when 30 V is applied. While this is only a simulation of the influence of voltage on the ion source, it shows that the voltage can make a significant difference in the function of the QMF.

It may be possible to reduce the effect of fringing fields by installing a grounded



(a) No voltage on the ion source.

(b) 15 volts on the ion source.



(c) 30 volts on the ion source.

Figure 3.3: Plots of the first 7 microseconds of ions exiting the ion source with initial conditions  $x_0 = 1$  mm,  $y_0 = 1$  mm,  $v_r/v_z = 0.05$ . Changing the voltage applied to the ion source significantly changes the trajectories.

copper mesh across the hole in the ground plate through which ions pass from the ion source into the QMF. An additional effect of this approach would be a slight reduction in ion current, as some would strike the mesh.

### 3.5 Potential QMF Modifications

As mentioned in section 3.1, though the QMF has produced much data and some conclusions have been drawn, we are still far from being able to use the quadrupole in our experiment to isolate a  ${}^7\text{Be}$  ion plasma. It is my purpose in this section to outline possible ways of improving the function of the quadrupole so that mass resolution can be achieved. I will cite the research that other groups have performed employing the use of a QMF. I will not delve into the full details of the research, but leave it to the reader to consult the sources mentioned.

Wexler [15](experimental) and Wagner [16](theory) used a quadrupole in an experiment with a cesium-uranium-fluoride plasma. Their work may be useful in our experiment because their plasma also had a high density, so they modeled the function of a QMF with a high density plasma. To improve the function of the quadrupole, Wexler and Wagner used a superimposed dipole field in conjunction with the normal quadrupole fields. It may be possible for something similar to be done in our experiment.

Konenkov et al. added auxiliary quadrupole excitation to improve performance of their QMF. [17] They used an additional AC voltage applied to the quadrupole to alter the shape of the stability curves, obtaining very precise regions of stability. Takahashi et al. used a Bessel-box type energy analyzer in a quadrupole. By altering the way that the ions enter the QMF from the ion source, they eliminated distracting noise from their experiment. [18] Tsukakoshi et al. used a zero-method control circuit

to apply voltages to their QMF. [19] Using this circuit, the voltages applied to the quadrupole could be specified with increased accuracy.

The important result of all this research is that it is possible to use a QMF in experiments similar to ours to obtain the desired results. Using previous research as a guide, it may be possible for us to modify our quadrupole to enable it to isolate a  ${}^7\text{Be}$  plasma.

## 3.6 Conclusion

While the QMF has been simulated and manufactured, we are still far from understanding it. We cannot yet operate the quadrupole accurately enough to use it in the experiment of measuring the half-life of ionized  ${}^7\text{Be}$ .

In future research of the QMF, it will be important to gain a good understanding of each component that contributes to the function of the quadrupole. The ion source must be analyzed so that its inconsistencies are understood. The DC and AC components of the voltages on the quadrupole must be made so that they can be applied without error. The magnetic field must be measured accurately and completely, and its effects on ions independent of the QMF must be understood.

There are a number of ways that the QMF may be understood enough to be used in the experiment. It may be possible to create simulations that more accurately reflect the behavior of the experimental quadrupole. It may also be possible to modify the experiment so that it more closely matches the conditions of my simulations. One method to accomplish this is reducing the current from the ion source to reduce the density of plasma in the quadrupole. Another option is to alter the function of the QMF as outlined in the previous section to make mass filtration possible.

It is hoped that understanding of the quadrupole will be obtained and the quadrupole

will be an essential part of the system that will measure the half-life of ionized  ${}^7\text{Be}$ . The measurement of this half-life will yield a better understanding of the variable decay rate of this isotope and the studies of which it is a part.

# Bibliography

- [1] C. W. Johnson, “The Fate of  ${}^7\text{Be}$  in the Sun,” *Astrophys. J.* **392**, 320–327 (1992).
- [2] M. Yoshimori, “Production and behavior of beryllium-7 radionuclide in the upper atmosphere,” *Adv. Space Res.* **36**, 922–926 (2005).
- [3] D. E. Walling, Q. He, and W. Blake, “Use of  ${}^7\text{Be}$  and  ${}^{137}\text{Cs}$  measurements to document short- and medium-term rates of water-induced soil erosion on agricultural land,” *Water Resour. Res.* **35**, 3865–3874 (1999).
- [4] D. Prime, V. Smith, and F. M. Ashworth, “Beryllium-7 in sheep,” *J. Radiol. Prot.* **8**, 239 (1988).
- [5] S. Wexler, E. K. Parks, C. E. Young, and R. A. Bennett, “Enhanced Electron-Capture Decay Rate of  ${}^7\text{Be}$  Encapsulated in  $\text{C}_{60}$  Cages,” *Phys. Rev. Lett.* **93**, 112501 (2004).
- [6] C. Huh, “Dependence of the decay rate of  ${}^7\text{Be}$  on chemical forms,” *Earth Planet. Sci. Lett.* **171**, 352 (2004).
- [7] L. Liu and C. Huh, “Effect of pressure on the decay rate of  ${}^7\text{Be}$ ,” *Earth Planet. Sci. Lett.* **180**, 163 (2000).
- [8] D. Olson, “Development of a MEVVA Based Beryllium-7 Plasma Source,” M.S. thesis (Brigham Young University, Provo, Utah, 2007).

- [9] D. Olson, “Construction and Characterization of a Specialized Malmberg-Penning Trap for Confinement of a Nonneutral Radionuclide Plasma,” Undergraduate senior thesis (Brigham Young University, Provo, Utah, 2005).
- [10] J. Rober T. McIver, “Trajectory Calculations for Axial Injection of Ions into a Magnetic Field: Overcoming the Magnetic Mirror Effect with an R.F. Quadrupole Lens,” *Int. J. Mass Spectrom. Ion Processes* **98**, 35–50 (1990).
- [11] R. March and R. Hughes, *Quadrupole Storage Mass Spectrometry* (Wiley, New York, 1988).
- [12] P. H. Dawson and N. R. Whetten, in *Advances in Electronics and Electron Physics*, L. Marton, ed., (Academic, New York, 1969).
- [13] D. R. Denison, “Operating parameters of a quadrupole in a grounded cylindrical housing,” *J. Vac. Sci. Technol.* **8**, 266–269 (1971).
- [14] R. L. Spencer, *Computational Physics 430: Partial Differential Equations* (Brigham Young University, Department of Physics and Astronomy, 2006).
- [15] S. Wexler, E. K. Parks, C. E. Young, and R. A. Bennett, “Behavior of Cs-UF ion-pair plasmas in radiofrequency quadrupole-dipole fields Experiment,” *J. Appl. Phys.* **54**, 1730–1754 (1983).
- [16] A. Wagner, “Behavior of Cs-UF ion-pair plasmas in radiofrequency quadrupole-dipole fields Theory,” *J. Appl. Phys.* **54**, 1755–1780 (1983).
- [17] N. Konenkov, L. Cousins, V. Baranov, and M. Sudakov, “Quadrupole mass filter operation with auxiliary quadrupolar excitation: theory and experiment,” *Int. J. Mass Spectrom. Ion Processes* **208**, 17–27 (2001).

- [18] N. Takahashi, T. Hayashi, H. Akimichi, and Y. Tuzi, “Development of the quadrupole mass spectrometer with the BesselBox type energy analyzer: Function of the energy analyzer in the partial pressure measurements,” *J. Vac. Sci. Technol. A* **19**, 1688–1692 (2001).
- [19] O. Tsukakoshi, T. Hayashi, K. Yamamuro, and M. Nakamura, “Development of a high precision quadrupole mass filter using the zero-method control circuit,” *Rev. Sci. Instrum.* **71**, 1332–1336 (2000).

# Appendix A

## The Mathieu Equation

The Mathieu equation is of great importance to the function of the quadrupole mass filter. Knowledge about how to operate the QMF is obtained from this equation. Much of this appendix is a summary of the analysis of March and Hughes. [11]

To arrive at the Mathieu equation for ion motion in a quadrupole field, we start with the potential experienced by an ion in a quadrupole field. The potential is

$$\phi = \frac{\phi_0}{r_0^2}(\lambda x^2 + \sigma y^2 + \gamma z^2) \quad (\text{A.1})$$

in which  $\lambda$ ,  $\sigma$ , and  $\gamma$  are weighting constants for the respective coordinates,  $\phi_0$  is the applied electric potential, and  $r_0$  is the inner radius of the quadrupole as shown in Fig. 2.4. The applied potential on the QMF is

$$\phi_0 = U - V \cos(\Omega t) \quad (\text{A.2})$$

When the potential experienced by the ion (Eq. A.1) is put in Poisson's equation (Eq. 2.3) with  $\rho = 0$ , the condition

$$\lambda + \sigma + \gamma = 0 \quad (\text{A.3})$$

is obtained. In the two-dimensional quadrupole case, the potential in the z direction is zero. Thus,  $\gamma = 0$  and the limitations on the weighting constants can be satisfied

if

$$\lambda = -\sigma = 1 \quad (\text{A.4})$$

Thus, the field expression becomes

$$\phi(x, y) = \frac{\phi_0}{r_0^2}(x^2 - y^2) \quad (\text{A.5})$$

We can put the expression for  $\phi_0$  (Eq. A.2) into Eq. A.5 and differentiate with respect to  $x$  and  $y$  to obtain a potential gradient in each direction,

$$\frac{\partial\phi}{\partial x} = \frac{2x}{r_0^2}(U - V\cos\Omega t) \quad (\text{A.6})$$

$$\frac{\partial\phi}{\partial y} = \frac{2y}{r_0^2}(U - V\cos\Omega t) \quad (\text{A.7})$$

The electrical force on the ion in each direction is the potential gradient multiplied by the charge. Force also equals mass times acceleration. Equating the expressions for the forces, we obtain

$$F_x = m \frac{d^2x}{dt^2} = \frac{2ex}{r_0^2}(U - V\cos\Omega t) \quad (\text{A.8})$$

$$F_y = m \frac{d^2y}{dt^2} = \frac{2ey}{r_0^2}(U - V\cos\Omega t) \quad (\text{A.9})$$

Thus, the equations of motion for a singly charged positive ion in a two-dimensional quadrupole field are

$$\frac{d^2x}{dt^2} + \frac{2e}{mr_0^2}(U - V\cos\Omega t)x = 0 \quad (\text{A.10})$$

$$\frac{d^2y}{dt^2} + \frac{2e}{mr_0^2}(U - V\cos\Omega t)y = 0 \quad (\text{A.11})$$

$$\frac{d^2z}{dt^2} = 0 \quad (\text{A.12})$$

The equations in the  $x$  and  $y$  directions resemble the second-order linear differential equation known as the Mathieu equation. Mathieu originally developed this equation while investigating the motions of a vibrating membrane. The canonical form of the equation is

$$\frac{d^2u}{d\xi^2} + (a_u - 2q_u \cos 2\xi) u = 0 \quad (\text{A.13})$$

with  $u$  representing one of the coordinate axes. If we change variables in Eq. A.10 and Eq. A.11 so that

$$\xi = \frac{\Omega t}{2} \quad (\text{A.14})$$

we can obtain

$$\frac{d^2x}{d\xi^2} = -\frac{8exU}{mr_0^2\Omega^2} + \frac{8exV \cos 2\xi}{mr_0^2\Omega^2} \quad (\text{A.15})$$

and the same for the  $y$  direction. If we define  $a_x$  and  $q_x$  such that

$$a_x = \frac{8eU}{mr_0^2\Omega^2} \quad (\text{A.16})$$

and

$$q_x = \frac{4eV}{mr_0^2\Omega^2} \quad (\text{A.17})$$

we obtain

$$\frac{d^2x}{d\xi^2} + (a_x - 2q_x \cos 2\xi) x = 0 \quad (\text{A.18})$$

and the same equation in the  $y$  direction. Note that the values for  $a$  and  $q$  are the same as those in Eq. 2.1 and Eq. 2.2. Equation A.18 is the canonical form of the Mathieu equation. Thus, we can consult the knowledge of this historically important equation which has been studied extensively to learn about the function of the QMF.

The stable, bounded solutions for the Mathieu equation are well known. Stable solutions in the  $x$  direction fit under the curve

$$a_{x0} = 1 - q - \frac{1}{8}q^2 + \frac{1}{64}q^3 + \frac{1}{1536}q^4 + \dots \quad (\text{A.19})$$

This curve, plotted for  $a = 0.7$  to  $a = 0.9$ , is on the right in Fig. 2.1. Meanwhile, stable solutions in the  $y$  direction fit under the curve

$$a_{y0} = \frac{1}{2}q^2 - \frac{7}{128}q^4 + \frac{29}{2304}q^6 + \dots \quad (\text{A.20})$$

This curve, plotted for  $a = 0$  to  $a = 0.7$ , is on the left in Fig. 2.1.

The stability curves for the ideal QMF come from the analysis of the well-known Mathieu equation.

# Appendix B

## MATLAB Code

My project required a significant amount of coding in MATLAB. Only the most important programs from my simulations are included here. With all of these files in a directory, ion motion in our quadrupole field can be simulated.

### B.1 Solving the Voltage Grid

This program creates a grid of voltages for a quadrupole with rods of a specified radius and length.

```
%Solve Laplace's equation to obtain a grid of voltage values
clear;
close all;

%Input the grid points for the three-dimensional grid
%Include more points in the z direction because it is longer
N=25;
Nx=N;
Ny=N;
Nz=3*Nx;

%Define the radii of the necessary parameters
%In our QMF, the central region has radius 2cm, and the radius of the
%rods is half of that
r0=0.02;
r1=.5*r0;
l0=0.1;           %The length from z=0 to the beginning of the quadrupole
l=.4;            %The length of the quadrupole
lengthz=.567;    %The length between the ion source and the ion trap
```

```

ltot=lengthz+.3; %Add 30 cm for wiggle room for computation

%Define the length (diameter) of computation
Lx=.1;    %Length in x of the computation region
Ly=.1;    %Length in y of the computation region
Lz=ltot;  %Length in z of the computation region

% Define the grids
dx=Lx/(Nx-1);    %X-grid spacing
dy=Ly/(Ny-1);    %Y-grid spacing
dz=Lz/(Nz-1);    %Z-grid spacing
x=(0:dx:Lx)-.5*Lx;    %X-grid, centered at x=0
y=(0:dy:Ly)-.5*Ly;    %Y-grid, centered at y=0
z=(0:dz:Lz);        %Z-grid, starting at one end of the quadrupole

%Determine the approximate best omega: parameter in SOR
omega=1.72;

%Set the error criterion
errortest=1e-6;

%Define the voltages
U1=1;          %Direct current potential
P1=U1;        %Potential for two of the poles
P2=-U1;       %Potential for the other two poles

%Define boundary conditions
%Put the boundary conditions in a matrix U
%Grounded around the outside edge
U=zeros(Nx,Ny,Nz);

%Define the mask
mask=zeros(Nx,Ny,Nz);
%Make the grounded border around the outside
for i=1:Nx
    for j=1:Ny
        r=sqrt(x(i)^2+y(j)^2);
        if r<(r0+2*r1)
            mask(i,j,:)=1;
        else mask(i,j,:)=0;
        end
    end
end

%Make the poles of the quadrupole

```

```

%Start with the left pole
%The center or the pole is r0 to the left
%of the center of the region
for i=1:Nx
    for j=1:Ny
        r=sqrt((x(i)+(r0+r1))^2+y(j)^2);
        if r<r1
            mask(i,j,:)=0;
            U(i,j,:)=P1;
        end
    end
end
%Now for the right pole
for i=1:Nx
    for j=1:Ny
        r=sqrt((x(i)-(r0+r1))^2+y(j)^2);
        if r<r1
            mask(i,j,:)=0;
            U(i,j,:)=P1;
        end
    end
end
%Now for the bottom pole
for i=1:Nx
    for j=1:Ny
        r=sqrt((y(j)+(r0+r1))^2+x(i)^2);
        if r<r1
            mask(i,j,:)=0;
            U(i,j,:)=P2;
        end
    end
end
%Now for the top pole
for i=1:Nx
    for j=1:Ny
        r=sqrt((y(j)-(r0+r1))^2+x(i)^2);
        if r<r1
            mask(i,j,:)=0;
            U(i,j,:)=P2;
        end
    end
end
%Now define the boundary conditions at the ends of the quadrupole
U(:, :, 1)=0;

```

```

U(:,:,Nz)=0;
mask(:,:,1)=0;
mask(:,:,Nz)=0;

%The quadrupole itself is only defined at the center of the region of
%computation: we are solving the fields for free space outside the
%quadrupole in the z direction
%Thus, we can limit U to be zero anywhere outside the middle 30cm of the
%computation region
%First, define the limits in the index region
%Also fix the mask so that it iterates all the regions without poles
Nz1=10;
Nz2=10+1;

for n=1:Nz
    if z(n)<Nz1
        U(:,:,n)=0;
        mask(:,:,n)=1;
    end
    if z(n)>Nz2
        U(:,:,n)=0;
        mask(:,:,n)=1;
    end
end

%Define the scale of the voltage, to be used to check the error in the
%iterations
Uscale=max(max(max(abs(U))));

%Now plug the initial condition matrix U into V
%to be manipulated by iteration to determine the fields
V=U;

%Set a maximum iteration count
Niter=Nx*Ny*Nz;

%Set factors used repeatedly in the algorithm
facyz=dy^2*dz^2;
facxz=dx^2*dz^2;
facxy=dx^2*dy^2;

for n=1:Niter
    err(n)=0;          %initialize the error at iteration n to zero
    for i=2:(Nx-1)    %Loop over interior points only
        for j=2:(Ny-1)

```

```

        for k=2:(Nz-1)
            if (mask(i,j,k))==1
                rhs=(facyz*(V(i+1,j,k)+V(i-1,j,k))+facxz*...
                    (V(i,j+1,k)+V(i,j-1,k))+facxy*...
                    (V(i,j,k+1)+V(i,j,k-1)))/...
                    (2*(facyz+facxz+facxy));
                err(n)=max(err(n),abs(V(i,j,k)-rhs)/Uscale);
                V(i,j,k)=omega*rhs+(1-omega)*V(i,j,k);
            end
        end
    end
end
if (abs(err(n)) < errortest)
    fprintf('After %g iterations, error= %g\n',n,err(n));
    disp('Desired accuracy achieved; breaking out of loop');
    break;
end
end

%make a surface plot
figure
surf(x,y,V(:,:,round(Nz/2))');
xlabel('x');ylabel('y');
title('Fields in the middle of the quadrupole')

%Make an animation of the fields as the z direction moves past the
%ends of the quadrupole
for m=1:Nz
    if z(m)>(l0+l-10/2)
        break
    end
end
for s=1:Nz
    if z(s)>(l0+l+10/2)
        break
    end
end
figure
for n=m:s
    surf(x,y,V(:,:,n))';
    zlim([-1 1])
    p=z(n)-(.3+3*(r0+2*r1));
    title(['Fields at ',num2str(p),' outside the quadrupole'])
    pause
end
end

```

```

%Display the maximum voltage at three points outside the quadrupole
v1=max(max(V(:,:,s-3)));
q=100*(z(s-3)-(z(s)+z(m))/2);
fprintf('Voltage %1.4gcm outside the quadrupole - %1.4g \n',q,v1)
v1=max(max(V(:,:,s)));
q=100*(z(s)-(z(s)+z(m))/2);
fprintf('Voltage %1.4gcm outside the quadrupole - %1.4g \n',q,v1)
v1=max(max(V(:,:,s+3)));
q=100*(z(s+3)-(z(s)+z(m))/2);
fprintf('Voltage %1.4gcm outside the quadrupole - %1.4g \n',q,v1)

%Make a one-dimensional cross section of the voltage
vt1=round(Nx/4);
vt2=round(Ny/2);
Vline=reshape(V(vt1,vt2,:),1,Nz);
figure
plot(z,Vline)

%Make a slice across the quadrupole
Vslice=V((Nx/2)+.5, :, round(Nz/2));
figure
plot(x,Vslice,'b-');
hold on
plot(r0,-1,'r*')
plot(r0+dx,-1,'r*')
plot(-r0,-1,'r*')
plot(-r0-dx,-1,'r*')

%Define the error in the radius measurement
for n2=round(Nx/6):round(Nx/2)
    if Vslice(n2)>-.99
        break
    end
end
xspecial=x(n2-1);
diff=abs(r0+xspecial);

%Save the data to be loaded in setup.m to solve for electric fields
save potential3coarse V x y z diff

```

## B.2 Solving the Electric Fields

This program is to be run after the previous program to solve for the electric fields in the quadrupole.

```

%Calculate the electric field from the potential in the x and y directions
%and load it into matrices Ex and Ey
clear;
close all;

load potential3coarse
xpot=x;
ypot=y;
zpot=z;

%Establish matrices for Ex, Ey, and Ez
Ex=zeros(length(x),length(y),length(z));
Ey=zeros(length(x),length(y),length(z));
Ez=zeros(length(x),length(y),length(z));

for n=2:length(x)-1
    for m=2:length(y)-1
        for k=2:length(z)-1
            Ex(n,m,k)=(V(n-1,m,k)-V(n+1,m,k))/(2*(x(n+1)-x(n)));
            Ey(n,m,k)=(V(n,m-1,k)-V(n,m+1,k))/(2*(y(m+1)-y(m)));
            Ez(n,m,k)=(V(n,m,k-1)-V(n,m,k+1))/(2*(z(k+1)-z(k)));
        end
    end
end

end

%Save the electric fields
save setupvar Ex Ey Ez xpot ypot zpot diff

```

### B.3 The Magnetic Field Values

This program gives the values for the magnetic field which were measured directly from the experimental system.

```

% This will define the axial magnetic field and necessary info to
% calculate the axial and radial field (near the axis)

global Zvalues Bzvalues dBzvalues;

% These values are the Bz calculated with a fully-corrected magnet using
% the experimental values for the flattest central field.

Zvalues=0:.01:1.1;

Bzvalues=[0.4295466304,0.4295662094,0.4295963200,0.4296345496,...
          0.4296763567,0.4297144393,0.4297378389,0.4297307893,...

```

```

0.4296713377,0.4295298046,0.4292671812,0.4288336081,...
0.4281670866,0.4271925686,0.4258215344,0.4239521532,...
0.4214701565,0.4182506079,0.4141605817,0.4090617099,...
0.4028094744,0.3952456023,0.3861851524,0.3754072203,...
0.3626580838,0.3476710715,0.3302084790,0.3101361090,...
0.2875384866,0.2628537666,0.2369436230,0.2109777410,...
0.1861265663,0.1632540784,0.1428023102,0.1248611022,...
0.1093023979,0.9589390572e-1,0.8437070998e-1,0.7447322880e-1,...
0.6596446198e-1,0.5863600761e-1,0.5230847743e-1,...
0.4682936807e-1,0.4206996264e-1,0.3792204876e-1,...
0.3429481525e-1,0.3111207999e-1,0.2830988893e-1,...
0.2583447768e-1,0.2364055984e-1,0.2168990148e-1,...
0.1995013867e-1,0.1839380060e-1,0.1699750108e-1,...
0.1574127219e-1,0.1460801272e-1,0.1358303204e-1,...
0.1265367221e-1,0.1180899351e-1,0.1103951398e-1,...
0.1033699044e-1,0.9694236812e-2,0.9104970776e-2,...
0.8563685486e-2,0.8065540777e-2,0.7606271621e-2,...
0.7182110507e-2,0.6789721112e-2,0.6426142183e-2,...
0.6088739303e-2,0.5775163515e-2,0.5483316050e-2,...
0.5211317625e-2,0.4957482239e-2,0.4720294228e-2,...
0.4498388514e-2,0.4290533437e-2,0.4095615636e-2,...
0.3912627056e-2,0.3740653115e-2,0.3578863421e-2,...
0.3426501954e-2,0.3282880101e-2,0.3147369297e-2,...
0.3019394995e-2,0.2898431358e-2,0.2783996687e-2,...
0.2675648590e-2,0.2572980875e-2,0.2475619731e-2,...
0.2383220755e-2,0.2295466419e-2,0.2212063618e-2,...
0.2132741446e-2,0.2057249063e-2,0.1985354278e-2,...
0.1916841724e-2,0.1851511590e-2,0.1789178204e-2,...
0.1729668832e-2,0.1672822884e-2,0.1618490556e-2,...
0.1566532107e-2,0.1516817414e-2,0.1469224744e-2,...
0.1423640175e-2,0.1379957460e-2,0.1338076844e-2,...
0.1297904846e-2,0.1259354042e-2];

NBvalues=length(Zvalues);

dBzvalues(2:NBvalues-1)=(Bzvalues(3:NBvalues)-Bzvalues(1:NBvalues-2))./...
    (Zvalues(3:NBvalues)-Zvalues(1:NBvalues-2));

dBzvalues(1)=3*dBzvalues(2)-3*dBzvalues(3)+dBzvalues(4);
dBzvalues(NBvalues)=3*dBzvalues(NBvalues-1)-3*dBzvalues(NBvalues-2)+...
    dBzvalues(NBvalues-3);

plot(Zvalues,Bzvalues);

figure

```

```

plot(Zvalues,dBzvalues);

save Bvalues Bzvalues dBzvalues Zvalues

```

## B.4 The Magnetic Field Grid

This program puts the magnetic field values into a grid that is the same size as the grid for the electric field.

```

clear;
close all;

%Load the values for the magnetic fields from Binit.m
load Bvalues
%Also load the variables from the electric field solver so we can get
%similar matrices to compare with the magnetic field matrices
load setupvar

%Start by changing the magnetic field values from Bvalues.m to values that
%correlate with the quadrupole
l0=0.1;           %The location of the mouth of the quadrupole
ltot=0.867;      %The length of the computation region
N=length(zpot);
dz=ltot/(N-1);
Bzpot=0:dz:ltot;

%Interpolate the magnetic fields onto the values that we need them for and
%plot the new values
Bzvaluesnew=interp1(Zvalues,Bzvalues,Bzpot);
subplot(2,2,1)
plot(Bzpot,Bzvaluesnew)
dBzvaluesnew=interp1(Zvalues,dBzvalues,Bzpot);
subplot(2,2,2)
plot(Bzpot,dBzvaluesnew)

%Reverse the direction of the magnetic fields and make the derivatives
%negative
zB=Bzvaluesnew(N:-1:1);
dzB=-dBzvaluesnew(N:-1:1);
subplot(2,2,3)
plot(Bzpot,zB)
subplot(2,2,4)
plot(Bzpot,dzB)

%Build matrices for the magnetic field values

```

```

Bz=zeros(length(xpot),length(ypot),length(zpot));
Bx=zeros(length(xpot),length(ypot),length(zpot));
By=zeros(length(xpot),length(ypot),length(zpot));

for k=1:N
    Bz(:, :,k)=zB(k);
    for i=1:length(xpot)
        for j=1:length(ypot)
            Bx(i,j,k)=-0.5*xpot(i)*dzB(k);
            By(i,j,k)=-0.5*ypot(j)*dzB(k);
        end
    end
end

save Bsetupvar Bx By Bz

```

## B.5 The Mover

This program must be in the same directory as the program in the next section in order for the motion of ions in the quadrupole to be simulated.

```

%Define the function for the ion motion
function F=quadfun3D(t,y)

%Declare pertinent variables to be global
global U V omega Ex Ey Ez xpot ypot zpot Bx By Bz ctm;

%Set up the function F
F=zeros(length(y),1);

%Define the system of first order differential equations
%Start with the equation related to the velocity
F(1)=y(2);
F(3)=y(4);
F(5)=y(6);

%Set the position as the result from the ode in the main editor
xpos=y(1);
ypos=y(3);
zpos=y(5);

%Solve for the electric fields at the actual position of the particle
Ex1=interp3(xpot,ypot,zpot,Ex,ypos,xpos,zpos,'linear',0);
Ey1=interp3(xpot,ypot,zpot,Ey,ypos,xpos,zpos,'linear',0);
Ez1=interp3(xpot,ypot,zpot,Ez,ypos,xpos,zpos,'linear',0);

```

```

%Interpolate for the magnetic fields at the actual position of the particle
Bx1=interp3(xpot,ypot,zpot,Bx,ypos,xpos,zpos,'linear',0);
By1=interp3(xpot,ypot,zpot,By,ypos,xpos,zpos,'linear',0);
Bz1=interp3(xpot,ypot,zpot,Bz,ypos,xpos,zpos,'linear',0);

%Now do the equation related to the position
F(2)=ctm*(Ex1*(U+V*cos(omega*t))+y(4)*Bz1-y(6)*By1);
F(4)=ctm*(Ey1*(U+V*cos(omega*t))-y(2)*Bz1+y(6)*Bx1);
F(6)=ctm*(Ez1*(U+V*cos(omega*t))+y(2)*By1-y(4)*Bx1);

```

## B.6 Solving the Ion Motion

This program is the end result file that is used in conjunction with uploaded variables and a function file to generate ion motion in the three-dimensional quadrupole.

```

clear; close all;

%declare global variables
global U V omega Ex Ey Ez Exp Eyp Ezp Exc Eyc Ezc ...
      xpot ypot zpot Bx By Bz r0 r1 ctm diff;

%Upload the electric fields from where we solved them in setup.m
load setupvar;

%Upload the magnetic fields from where we solved them in Bvars.m
load Bsetupvar;

%Change the magnetic field strength as desired
Bfactor=1;
Badd=0;
Bz=Bfactor*Bz+Badd;
Bx=Bfactor*Bx;
By=Bfactor*By;

%Change the fringing field as desired:
%Efactor=1 is the effect of one volt applied to the ion source
Efactor=30;
Exp=Efactor*Exp;
Eyp=Efactor*Eyp;
Ezp=Efactor*Ezp;

%Change the charged plate field as desired:
%Ecfactor=1 is the effect of 10-9 Coulombs of charge on the support plate
Ecfactor=.05;

```

```

Exc=Ecfactor*Exc;
Eyc=Ecfactor*Eyc;
Ezc=Ecfactor*Ezc;

%set values for global variables
q=1;           %charge of the ion in electron units
m=7.06;       %mass of ion: mass of beryllium 7 ion in amu is 7.06
r0=0.02;      %inner radius of quadrupole
r0p=r0+diff;  %account for the effects of the grid
f=5.5e5;      %frequency of the RF voltage
omega=2*pi*f; %angular frequency of the RF voltage
r1=.5*r0;     %The radius of individual quadrupole poles
l0=0.1;       %the distance from z=0 to where the quadrupole starts
l=.4;         %The length of the quadrupole
ltot=.567;    %The length between the ion source and the ion trap

%convert to SI units
charge=1.602e-19*q;
q=charge;
m=1.66e-27*m;
ctm=q/m;

%Define adjustable variables for modified stability curve
B=.001;
C=0.089;

%define U and V by the stability curve for a and q
qval=.72;
if qval<=.7624
    aval=.5*qval^2-(7/128)*qval^4+(29/2304)*qval^6;
    aval=B+aval;
else
    aval=1-(qval-C)-.125*(qval-C)^2+(1/64)*(qval-C)^3+(1/1536)*(qval-C)^4;
end

%The following lines are all for adjustments to a and q to test stability
aval=aval-.025;
% qval=qval-.001;
% qval=.65;
% aval=.17;

U=(aval*m*omega^2*r0p^2)/(8*q);
V=(qval*m*omega^2*r0p^2)/(4*q);
% omega=(2/r0p)*sqrt((q*V)/(qval*m));
f=omega/(2*pi);

```

```

%Change the AC, DC fields as desired
Ufactor=1;
Vfactor=1;
U=U*Ufactor;
V=V*Vfactor;

%Define initial conditions by three parameters, ratio of radial velocity to
%longitudinal velocity, azimuthal angle, and distance from quadrupole
vr vz=.053; %ratio of radial velocity to longitudinal velocity
theta=(pi)/4; %initial angle from the x axis
d=.02; %distance the ion source is set back from the quadrupole

%Define the total velocity of the particle
v=2.5e4;

%Define initial conditions vector
y0=zeros(6,1);

%Set initial conditions
x0pos=.001;
y0pos=.001;
z0pos=10-d;
vx0=(((1/vr vz)^2+1)^(-1/2))*v*cos(theta);
vy0=(((1/vr vz)^2+1)^(-1/2))*v*sin(theta);
vz0=((vr vz^2+1)^(-1/2))*v;

%set the start and end times
tstart=0;
tfinal=25e-6;

y0(1)=x0pos; %initial x position
y0(2)=vx0; %initial x velocity
y0(3)=y0pos; %initial y position
y0(4)=vy0; %initial y velocity
y0(5)=z0pos; %initial z position
y0(6)=vz0; %initial z velocity

%set options for tolerance
options=odeset('RelTol',1e-5);

%solve the equations for the ion motion
[t,y]=ode45(@quadfun3D,[tstart,tfinal],y0,options);

%Separate into components

```

```

x1=y(:,1);
vx=y(:,2);
y1=y(:,3);
vy=y(:,4);
z1=y(:,5);
vz=y(:,6);

%separate the components: don't plot what goes out of the quadrupole
for n=1:length(x1)
    xp(n)=y(n,1);
    if sqrt(x1(n)^2+y1(n)^2) > (r0+.001)
        break
    end
end
vxp=vx(1:length(xp));
yp=y1(1:length(xp));
vyp=vy(1:length(xp));
zp=z1(1:length(xp));
vzp=vz(1:length(xp));
xp=xp';
t1=t(1:length(xp));

%define and plot the quadrupole poles in two dimensions
x2=-r1:r1/100:r1;
y2=real((r1^2-x2.^2).^(1/2)+r0+r1);
y3=-y2;
plot(x2,y2,'r-',x2,y3,'r-')
hold on
y4=real((r1^2-x2.^2).^(1/2)-r0-r1);
y5=-y4;
plot(x2,y4,'r-',x2,y5,'r-')
x3=-r0-2*r1:r1/100:-r0;
y6=real((r1^2-(x3+r0+r1).^2).^(1/2));
y7=-y6;
plot(x3,y6,'r-',x3,y7,'r-')
x4=r0:r1/100:r0+2*r1;
y8=real((r1^2-(x4-r0-r1).^2).^(1/2));
y9=-y8;
plot(x4,y8,'r-',x4,y9,'r-')
plot(r0+r1,0,'r*',-r0-r1,0,'r*',0,r0+r1,'r*',0,-r0-r1,'r*');

%plot x versus y
plot(xp,yp);
xlabel('x'); ylabel('y');
axis equal

```

```

ylim([- .025 .025])

%Find and prepare to plot the point where the B-field is half maximum
Bfieldmax=max(max(max(Bz)));
for n7=1:length(zpot)
    Bmaxtemp=max(max(Bz(:,:,n7)));
    if Bmaxtemp>.5*Bfieldmax
        break
    end
end

%define and plot the quadrupole poles in three dimensions
figure
x2=-r1:r1/100:r1;
y2=real((r1^2-x2.^2).^(1/2)+r0+r1);
y3=-y2;
zc1=zeros(1,length(x2));
zc1(:)=l0;
zc2=zeros(1,length(x2));
zc2(:)=(l+2*10)/2; %Distance to the middle of the quadrupole
zc3=zeros(1,length(x2));
zc3(:)=l0+l; %Distance to the end of the quadrupole
zc4=zeros(1,length(x2));
zc4(:)=ltot;
plot3(x2,y2,zc1,'r-',x2,y3,zc1,'r-')
hold on
plot3(x2,y2,zc2,'r-',x2,y3,zc2,'r-')
plot3(x2,y2,zc3,'r-',x2,y3,zc3,'r-')
plot3(x2,y2,zc4,'r-',x2,y3,zc4,'r-')
y4=real((r1^2-x2.^2).^(1/2)-r0-r1);
y5=-y4;
plot3(x2,y4,zc1,'r-',x2,y5,zc1,'r-')
plot3(x2,y4,zc2,'r-',x2,y5,zc2,'r-')
plot3(x2,y4,zc3,'r-',x2,y5,zc3,'r-')
plot3(x2,y4,zc4,'r-',x2,y5,zc4,'r-')
x3=-r0-2*r1:r1/100:-r0;
y6=real((r1^2-(x3+r0+r1).^2).^(1/2));
y7=-y6;
plot3(x3,y6,zc1,'r-',x3,y7,zc1,'r-')
plot3(x3,y6,zc2,'r-',x3,y7,zc2,'r-')
plot3(x3,y6,zc3,'r-',x3,y7,zc3,'r-')
plot3(x3,y6,zc4,'r-',x3,y7,zc4,'r-')
x4=r0:r1/100:r0+2*r1;
y8=real((r1^2-(x4-r0-r1).^2).^(1/2));
y9=-y8;

```

```

plot3(x4,y8,zc1,'r-',x4,y9,zc1,'r-')
plot3(x4,y8,zc2,'r-',x4,y9,zc2,'r-')
plot3(x4,y8,zc3,'r-',x4,y9,zc3,'r-')
plot3(x4,y8,zc4,'r-',x4,y9,zc4,'r-')
rf1=r0+r1;
rf2=-rf1;
plot3([rf1 rf1],[0 0],[10 10+1],'r-',[rf2 rf2],[0 0],[10 10+1],'r-');
plot3([0 0],[rf1 rf1],[10 10+1],'r-',[0 0],[rf2 rf2],[10 10+1],'r-');
%Plot an 'x' where the B-field is at half maximum
plot3([0 0],[rf1 rf2],[zpot(n7) zpot(n7)],'g-');
plot3([rf1 rf2],[0 0],[zpot(n7) zpot(n7)],'g-');
%Plot an 'x' where the flange is
plot3([0 0],[rf1 rf2],[0.135 0.135],'g-');
plot3([rf1 rf2],[0 0],[0.135 0.135],'g-');

%Plot the motion in three dimensions
plot3(xp,yp,zp)
axis equal

%Plot the representative stability curves and region we are testing
figure
q=0:.05:.8;
a=.5*q.^2-(7/128)*q.^4+(29/2304)*q.^6;
q1=.65:.01:.9;
a1=1-q1-.125*q1.^2+(1/64)*q1.^3+(1/1536)*q1.^4;
plot(q,a,'r-',q1,a1,'r-')
hold on
plot(qval,aval,'r*')
xlabel('q');ylabel('a');
title('Testing Be-7 for Stability')
qp=q;
ap=.5*qp.^2-(7/128)*qp.^4+(29/2304)*qp.^6;
ap=B+ap;
q1p=q1+C;
a1p=a1;
plot(qp,ap,'b-',q1p,a1p,'b-')
plot(qval,aval,'b*')
plot([0 qval],[0 aval],'b-')
plot([qval (1/qval)*qval],[aval (1/qval)*aval],'b-')

```

# Appendix C

## Machining Drawings

This section includes the drawings which were used to fabricate the parts for the quadrupole and support structure. Each of these pieces are part of the overall system shown in Fig. 2.11.

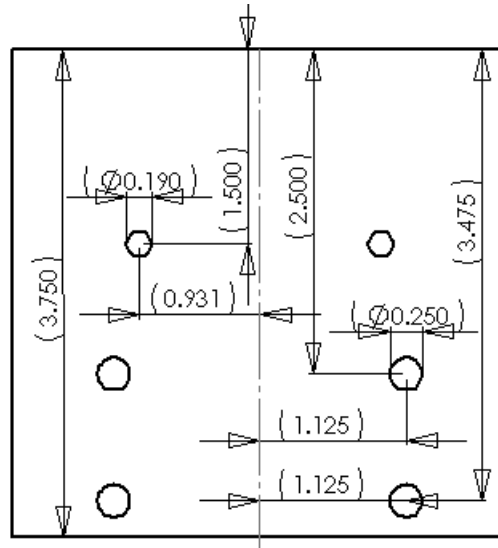


Figure C.1: The plate that sits in the bottom of the system. The holes are where the bracket for the ion source (Fig. C.2 and Fig. C.3) and ground plate (Fig. C.4) are attached. All dimensions shown are in units of inches.

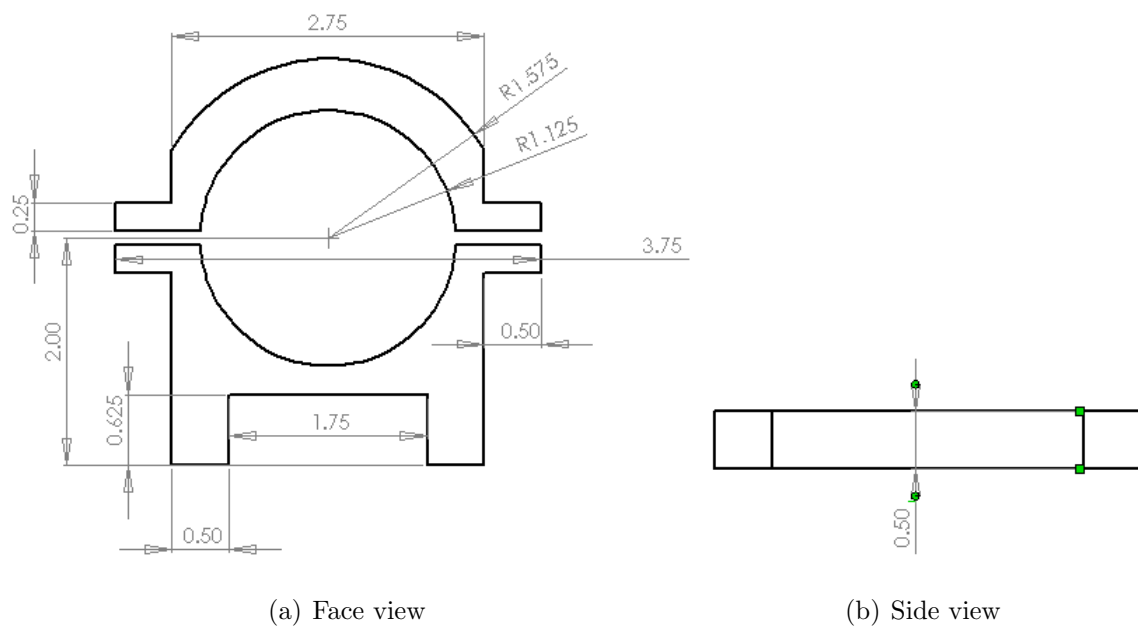
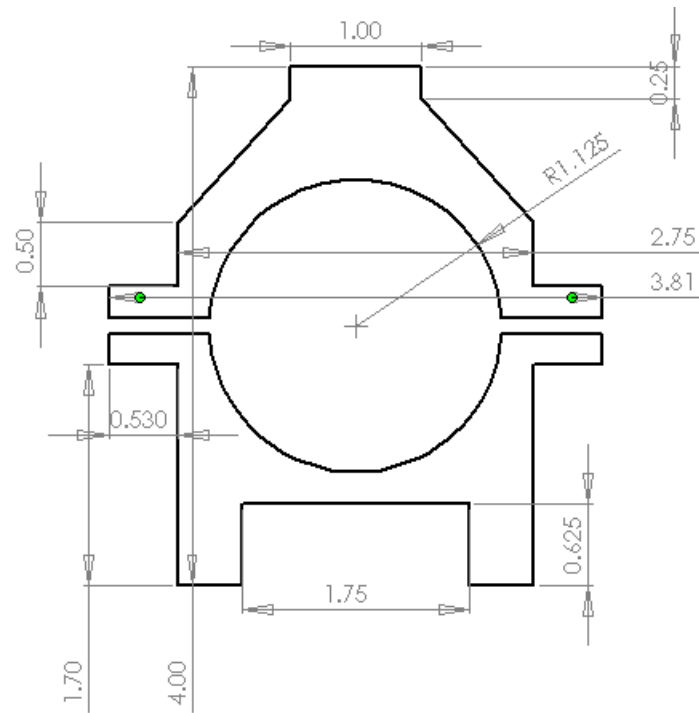
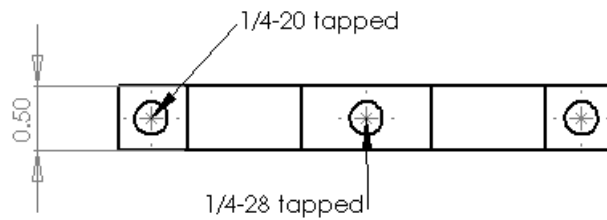


Figure C.2: The bracket that holds the ion source in place that is furthest from the QMF. All dimensions shown are in units of inches.



(a) Face view



(b) Side view

Figure C.3: The bracket that holds the ion source in place that is closest to the QMF.

All dimensions shown are in units of inches.

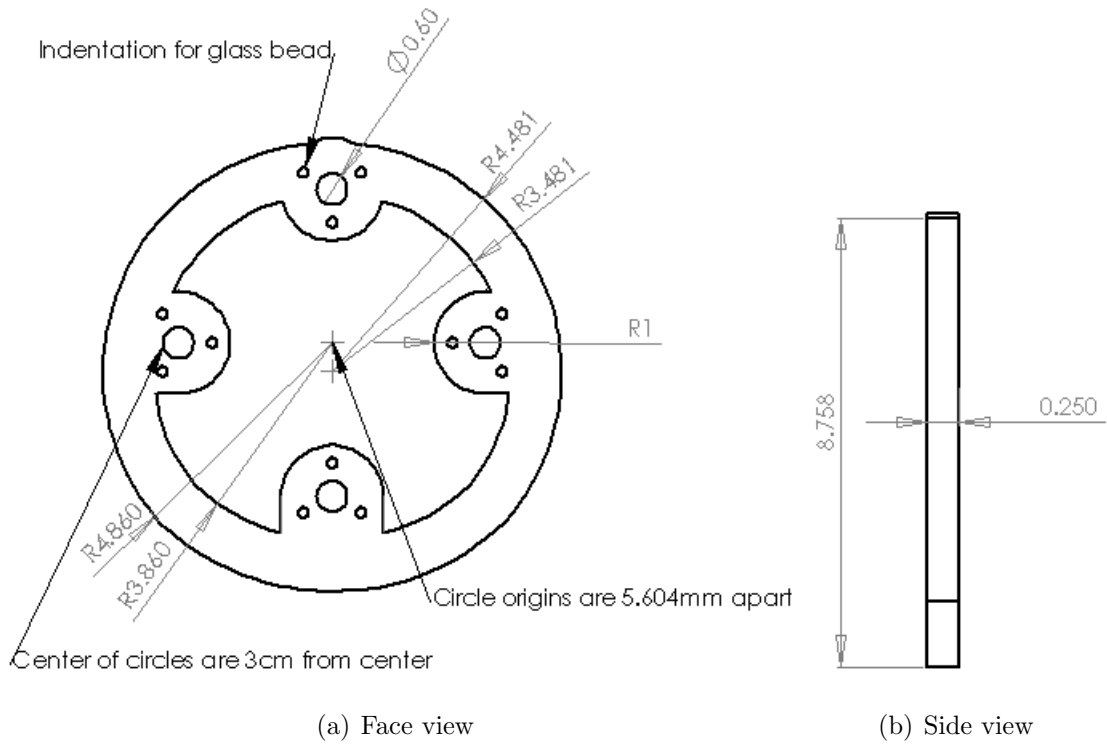


Figure C.4: The ground plate located between the ion source and the QMF. All dimensions shown are in units of centimeters.

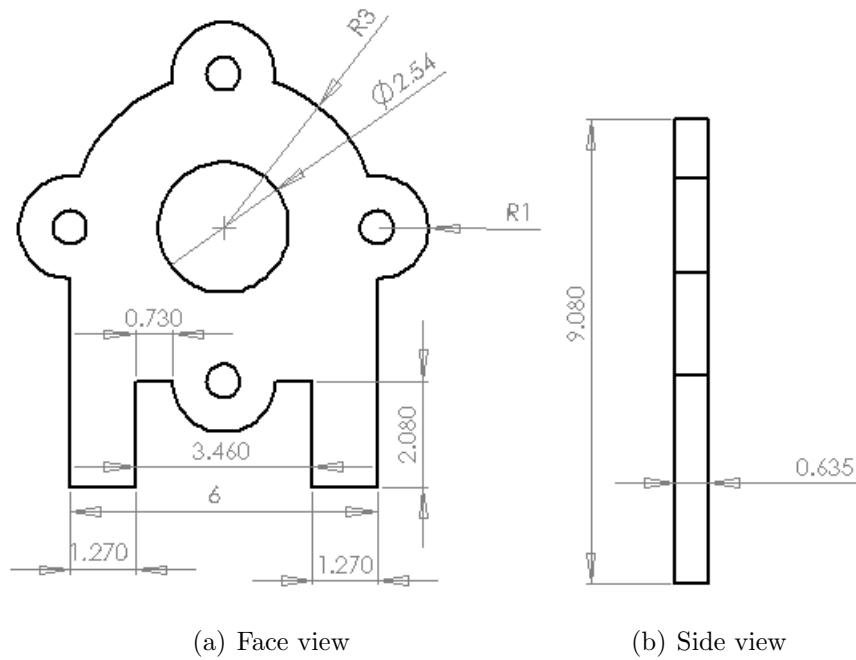


Figure C.5: The support at the end of the QMF closest to the ion source. The bottom radius is larger than the top radius to enable the piece to sit flush to the surface of the pipe in which it sits, while allowing the piece to be inserted in the pipe past welds connecting pieces of the pipe. All dimensions shown are in units of centimeters.

# Appendix D

## Pictures

This section includes some images of the actual experimental system.

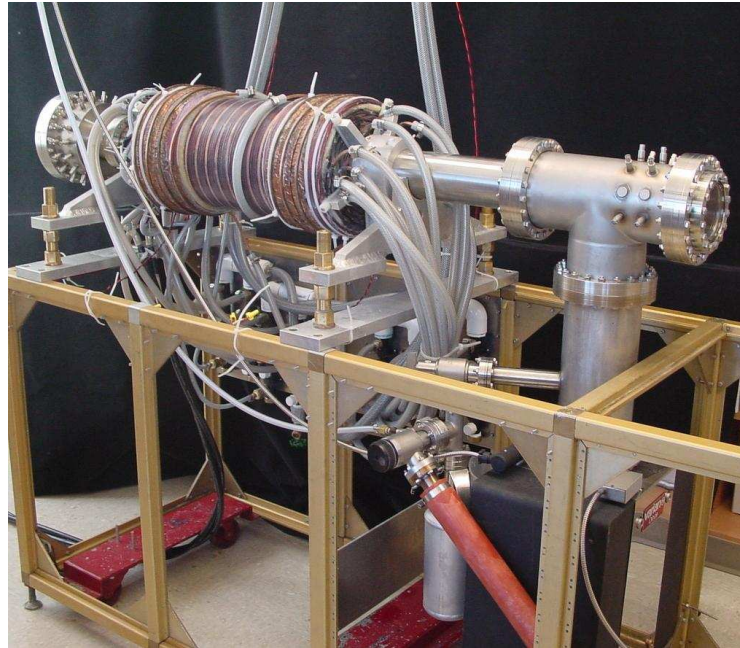


Figure D.1: Our experimental system. This picture is equivalent to the schematic of the system, Fig. 1.1. However, the actual picture is inverted left to right from the schematic. In the picture, the ion source is housed within the “T” on the right. The quadrupole is in the region between the “T” on the left and the ion trap on the right. The vacuum pump is the black box on the bottom right. The white plastic tubes are used to pump water through to cool the coils for the magnet.



Figure D.2: The completed quadrupole. Originally, the poles and the support piece at the far left in the picture were aluminum.

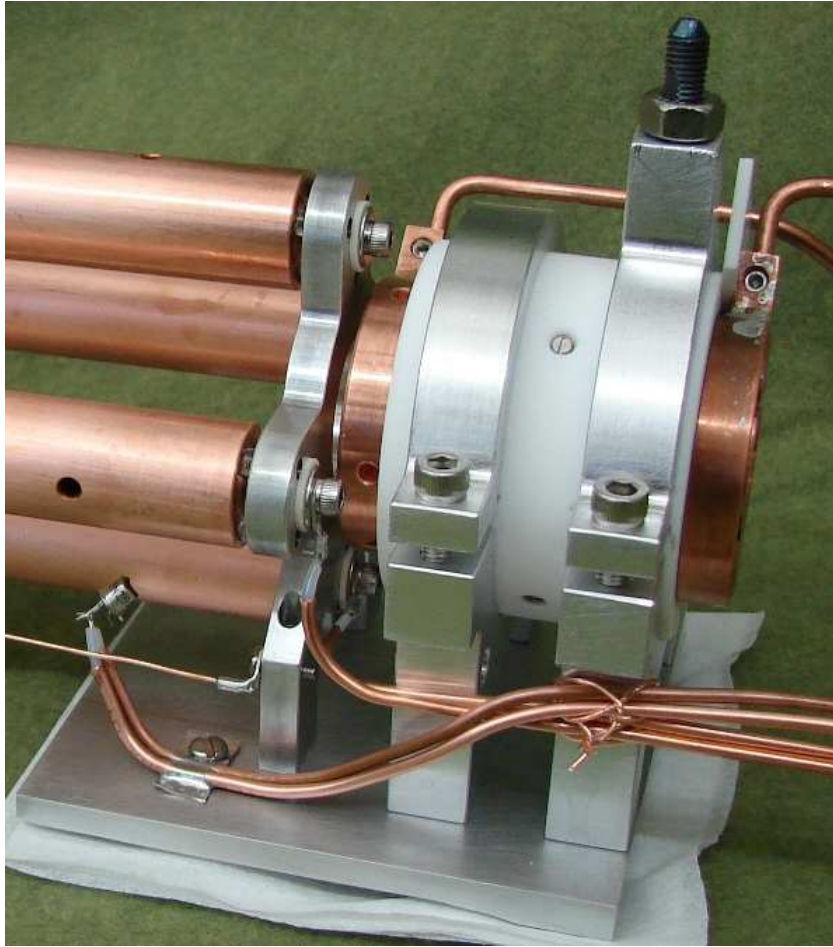


Figure D.3: A close up view of the ion source and quadrupole mounted in place. A photodiode is mounted on the left below the quadrupole. The quadrupole is mounted so that it is electrically insulated from the ground plate.

# Index

- aluminum oxide, 8, 31
- auxiliary quadrupole excitation, 36
- beryllium-7, 1, 13
- boron carbide, 3
- buckyball, 2
- charge collectors, 4, 29, 31
- copper, 31, 36
- cyclotron frequency, 22
- Debye length, 30
- dipole field, 36
- drawings, 62
- electric fields, 18
- electron capture, 2
- fringing fields, 34
- FTICR-MS, 4
- hyperbolic surfaces, 13
- ideal QMF, 9
- ion source, 3, 19, 26, 29, 34, 62
- isotopes of beryllium, 1
- magnetic field, 5, 19, 33
- magnetic mirror effect, 22
- Malmberg-Penning trap, 4
- Mathieu equation, 11, 17, 42
- MATLAB, 17, 46
- nano, 33
- particle-in-cell, 30
- plasma, 3, 29, 36
- Poisson's equation, 17
- ponderomotive force, 11
- QMF, geometry of, 11
- QMF, parameters of, 11
- resonance, 23
- sheep, 1
- soil erosion, 1
- SolidWorks, 6, 26, 62
- stability curves, 12
- successive over-relaxation (SOR), 18
- vacuum, 15, 26

Van de Graff accelerator, 3

voltage applied to QMF, 5, 12, 25, 36

zero-method control circuit, 36